

UC Irvine

UC Irvine Previously Published Works

Title

The effect of Nipbl haploinsufficiency on genome-wide cohesin binding and target gene expression

Permalink

<https://escholarship.org/uc/item/12t5689r>

Journal

BIOCHEMISTRY AND CELL BIOLOGY-BIOCHIMIE ET BIOLOGIE CELLULAIRE, 91(6)

ISSN

0829-8211

Authors

Chen, Yen-Yun
Chien, Richard
Newkirk, Daniel A
[et al.](#)

Publication Date

2013


Peer reviewed

RESEARCH

Open Access



The effect of Nipped-B-like (Nipbl) haploinsufficiency on genome-wide cohesin binding and target gene expression: modeling Cornelia de Lange syndrome

Daniel A. Newkirk^{1,2†}, Yen-Yun Chen^{1,6†}, Richard Chien^{1,7†}, Weihua Zeng^{1,8}, Jacob Biesinger^{2,9}, Ebony Flowers^{1,5,10}, Shimako Kawachi³, Rosaysela Santos³, Anne L. Calof³, Arthur D. Lander⁴, Xiaohui Xie^{2*} and Kyoko Yokomori^{1*} 

Abstract

Background: Cornelia de Lange syndrome (CdLS) is a multisystem developmental disorder frequently associated with heterozygous loss-of-function mutations of *Nipped-B-like* (*NIPBL*), the human homolog of *Drosophila Nipped-B*. *NIPBL* loads cohesin onto chromatin. Cohesin mediates sister chromatid cohesion important for mitosis but is also increasingly recognized as a regulator of gene expression. In CdLS patient cells and animal models, expression changes of multiple genes with little or no sister chromatid cohesion defect suggests that disruption of gene regulation underlies this disorder. However, the effect of *NIPBL* haploinsufficiency on cohesin binding, and how this relates to the clinical presentation of CdLS, has not been fully investigated. *Nipbl* haploinsufficiency causes CdLS-like phenotype in mice. We examined genome-wide cohesin binding and its relationship to gene expression using mouse embryonic fibroblasts (MEFs) from *Nipbl*^{+/-} mice that recapitulate the CdLS phenotype.

Results: We found a global decrease in cohesin binding, including at CCCTC-binding factor (CTCF) binding sites and repeat regions. Cohesin-bound genes were found to be enriched for histone H3 lysine 4 trimethylation (H3K4me3) at their promoters; were disproportionately downregulated in *Nipbl* mutant MEFs; and displayed evidence of reduced promoter-enhancer interaction. The results suggest that gene activation is the primary cohesin function sensitive to *Nipbl* reduction. Over 50% of significantly dysregulated transcripts in mutant MEFs come from cohesin target genes, including genes involved in adipogenesis that have been implicated in contributing to the CdLS phenotype.

Conclusions: Decreased cohesin binding at the gene regions is directly linked to disease-specific expression changes. Taken together, our *Nipbl* haploinsufficiency model allows us to analyze the dosage effect of cohesin loading on CdLS development.

Keywords: CdLS, Cohesin, *Nipbl*, Haploinsufficiency, Chromatin immunoprecipitation (ChIP), Gene regulation, Chromatin interaction, Chromatin regulation, Adipogenesis

* Correspondence: xhx@uci.edu; kyokomor@uci.edu

†Equal contributors

²Department of Computer Sciences, University of California, Irvine, CA 92697, USA

¹Department of Biological Chemistry, School of Medicine, University of California, Irvine, CA 92697, USA

Full list of author information is available at the end of the article



Background

CdLS (OMIM 122470, 300590, 610759) is a dominant genetic disorder estimated to occur in 1 in 10,000 individuals, characterized by facial dysmorphism, hirsutism, upper limb abnormalities, cognitive retardation, and growth abnormalities [1, 2]. Mutations in the *NIPBL* gene are linked to more than 55% of CdLS cases [3, 4]. *NIPBL* is an evolutionarily conserved, essential protein that is required for chromatin loading of cohesin [5]. Cohesin is a multiprotein complex, also conserved and essential, which functions in chromosome structural organization important for genome maintenance and gene expression [6–8]. Mutations in the cohesin subunits *SMC1* (human *SMC1* (*hSMC1*), *SMC1A*) and *hSMC3* were also found in a minor subset of clinically milder CdLS cases (~5% and <1%, respectively) [9–11]. More recently, mutation of *HDAC8*, which regulates cohesin dissociation from chromatin in mitosis, was found in a subset of CdLS patients (OMIM 300882) [12]. Mutations in the non-SMC cohesin component *Rad21* gene have also been found in patients with a CdLS-like phenotype (OMIM 606462), with much milder cognitive impairment [13]. Thus, mutations of cohesin subunits and regulators of cohesin's chromatin association cause related phenotypes, suggesting that impairment of the cohesin pathway makes significant contributions to the disease [2, 14].

The most common cause of CdLS is *NIPBL* haploinsufficiency [2, 15, 16]. Even a 15% decrease in expression was reported to cause mild but distinct CdLS phenotype, suggesting the extreme sensitivity of human development to *NIPBL* gene dosage [17, 18]. Similarly, *Nipbl* heterozygous mutant (*Nipbl*^{+/-}) mice display only a 25–30% decrease in *Nipbl* transcripts, presumably due to compensatory up-regulation of the intact allele [19]. They, however, exhibit wide-ranging defect characteristic of the disease, including small size, craniofacial anomalies, microbrachycephaly, heart defects, hearing abnormalities, low body fat, and delayed bone maturation [19]. Thus, these results indicate a conserved high sensitivity of mammalian development to *Nipbl* gene dosage and that *Nipbl*^{+/-} mice can serve as a CdLS disease model.

Although a canonical function of cohesin is sister chromatid cohesion critical for mitosis [8], a role for cohesin in gene regulation has been argued for based on work in multiple organisms [20, 21]. The partial decrease of *Nipbl* expression in CdLS patients and *Nipbl*^{+/-} mice was not sufficient to cause a significant sister chromatid cohesion defect or abnormal mitosis [19, 22–24]. Instead, a distinctive profile of gene expression changes was observed, revealing dosage-sensitive functional hierarchy of cohesin and strongly suggesting that transcriptional dysregulation underlies the disease phenotype [6, 18, 19, 25]. In *Nipbl*^{+/-} mutant mice, expression of many genes were affected,

though mostly minor, raising the possibility that small expression perturbations of multiple genes collectively contribute to the disease phenotype [19]. Indeed, combinatorial partial depletion of key developmental genes dysregulated in this mouse model successfully recapitulated specific aspects of the CdLS-like phenotype in zebrafish [26]. A recent study on CdLS patient lymphoblasts and correlation with *NIPBL* ChIP-seq revealed dysregulation of RNA processing genes, which also explains a certain aspect of CdLS cellular phenotype [27]. However, discordance of *NIPBL* and cohesin binding patterns in mammalian genome suggests that *NIPBL* may have cohesin-independent transcriptional effects [28]. Thus, it is important to determine the effects of *Nipbl* haploinsufficiency on cohesin binding and cohesin-bound target genes. While a similar study has been done using patient and control cells [18], the *Nipbl*^{+/-} mouse model in comparison with the *Nipbl*^{+/+} wild type provides an ideal isogenic system for this purpose.

Cohesin is recruited to different genomic regions and affects gene expression in different ways in mammalian cells [6, 7, 29]. In mammalian cells, one major mechanism of cohesin-mediated gene regulation is through CTCF [30–33]. CTCF is a zinc finger DNA-binding protein and was shown to act as a transcriptional activator/repressor as well as an insulator [34]. Genome-wide chromatin immunoprecipitation (ChIP) analyses revealed that a significant number of cohesin-binding sites overlap with those of CTCF in human and mouse somatic cells [30, 31]. Cohesin is recruited to these sites by CTCF and mediates CTCF's insulator function by bridging distant CTCF sites at, for example, the *H19/IGF2*, *IFN γ* , apolipoprotein, and β -globin loci [30, 31, 33, 35–38]. While CTCF recruits cohesin, it is cohesin that plays a primary role in long-distance chromatin interaction [36]. A more recent genome-wide Chromosome Conformation Capture Carbon Copy (5C) study revealed that CTCF/cohesin tends to mediate long-range chromatin interactions defining megabase-sized topologically associating domains (TADs) [39], indicating that CTCF and cohesin together play a fundamental role in chromatin organization in the nucleus. Cohesin also binds to other genomic regions and functions in a CTCF-independent manner in gene activation by facilitating promoter-enhancer interactions together with Mediator [35, 39–41]. Significant overlap between cohesin at non-CTCF sites and cell type-specific transcription factor-binding sites was found, suggesting a role for cohesin at non-CTCF sites in cell type-specific gene regulation [41–43]. In addition, cohesin is recruited to heterochromatic repeat regions [44, 45]. To what extent these different modes of cohesin recruitment and function are affected by *NIPBL* haploinsufficiency in CdLS has not been examined.

Here, using MEFs derived from *Nipbl*^{+/-} mice, we analyzed the effect of *Nipbl* haploinsufficiency on cohesin-

mediated gene regulation and identified cohesin target genes that are particularly sensitive to partial reduction of Nipbl. Our results indicate that Nipbl is required for cohesin binding to both CTCF and non-CTCF sites, as well as repeat regions. Significant correlation was found between gene expression changes in Nipbl mutant cells and cohesin binding to the gene regions, in particular promoter regions, suggesting that even modest Nipbl reduction directly and significantly affects expression of cohesin-bound genes. Target genes are enriched for developmental genes, including multiple genes that regulate adipogenesis, which is impaired in Nipbl^{+/-} mice [19]. The results indicate that Nipbl regulates a significant number of genes through cohesin. While their expression levels vary in wild type cells, the Nipbl/cohesin target genes tend on the whole to be downregulated in Nipbl mutant cells, indicating that Nipbl and cohesin are important for activation of these genes. Consistent with this, these genes are enriched for H3 lysine 4 trimethylation (H3K4me3) at the promoter regions. The long-distance interaction of the cohesin-bound promoter and a putative enhancer region is decreased by Nipbl reduction, indicating that reduced cohesin binding by Nipbl haploinsufficiency affects chromatin interactions. Collectively, the results reveal that Nipbl haploinsufficiency globally reduces cohesin binding, and its major transcriptional consequence is the downregulation of cohesin target genes.

Methods

Cells and antibodies

Mouse embryonic fibroblasts (MEFs) derived from E15.5 wild type and *Nipbl* mutant embryos were used as described previously [19]. In brief, mice heterozygous for *Nipbl* mutation were generated (*Nipbl*^{+/-}) from genetrapped ES cells. This mutation resulted in a net 30–50% decrease in *Nipbl* transcripts in the mice, along with many phenotype characteristics of human CdLS patients [19]. Wild type and mutant MEF cell lines derived from the siblings were cultured at 37 °C and 5% CO₂ in DMEM (Gibco) supplemented with 10% fetal bovine serum and penicillin-streptomycin (50 U/mL). Antibodies specific for hSMC1 and Rad21 were previously described [46]. Rabbit polyclonal antibody specific for the NIPBL protein was raised against a bacterially expressed recombinant polypeptide corresponding to the C-terminal fragment of NIPBL isoform A (NP_597677.2) (amino acids 2429–2804) [45]. Anti-histone H3 rabbit polyclonal antibody was from Abcam (ab1791).

ChIP-sequencing (ChIP-seq) and ChIP-PCR

ChIP was carried out as described previously [35]. Approximately 50 µg DNA was used per IP. Cells were crosslinked 10 min with 1% formaldehyde, lysed, and

sonicated using the Bioruptor from Diagenode to obtain ~200 bp fragments using a 30 s on/off cycle for 1 h. Samples were diluted and pre-cleared for 1 h with BSA and Protein A beads. Pre-cleared extracts were incubated with Rad21, Nipbl, and preimmune antibodies overnight. IP was performed with Protein A beads with subsequent washes. DNA was eluted off beads, reversed crosslinked for 8 h, and purified with the Qiagen PCR Purification Kit. Samples were submitted to Ambry Genetics (Aliso Viejo, CA) for library preparation and sequencing using the Illumina protocol and the Illumina Genome Analyzer (GA) system. The total number of reads before alignment were preimmune IgG, 7,428,656; Rad21 in control WT, 7,200,450; Rad21 in Nipbl^{+/-}, 4,668,622; histone H3 in WT, 26,630,000; and histone H3 in Nipbl^{+/-}, 24,952,439. Sequences were aligned to the mouse mm9 reference genome using Bowtie (with parameters -n2, -k20, -best, -strata, -chunkmbs 384) [47]. ChIP-seq data is being submitted to GEO. PCR primers used for manual ChIP confirmation are listed in Table 1. Primers corresponding to repeat sequences (major and minor satellite, rDNA, and SINEB1 repeats) were from Martens et al. [48]. For manual ChIP-PCR analysis of selected genomic locations, ChIP signals were normalized with preimmune IgG and input DNA from each cell sample as previously described [35, 45, 49]. The experiments were repeated at least three times using MEF samples from different litters, which yielded consistent results. PCR reactions were done in duplicates or triplicates.

Peak finding

Peaks were called using AREM (Aligning ChIP-seq Reads using Expectation Maximization) as previously described [50]. AREM incorporates sequences with one or many mappings to call peaks as opposed to using only uniquely mapping reads, allowing one to call peaks normally missed due to repetitive sequence. Since many peaks for Rad21 as well as CTCF can be found in repetitive sequence [50, 51], we used a mixture model to describe the data, assuming $K + 1$ clusters of sequences (K peaks and background). Maximum likelihood is used to estimate the locations of enrichment, with the read alignment probabilities iteratively updated using EM. Final peaks are called for each window assuming a Poisson distribution, calculating a p value for each sequence cluster. The false discovery rate for all peaks was determined relative to the pre-immune sample, with EM performed independently for the pre-immune sample as well. Full algorithm details are available, including a systematic comparison to other common peak callers such as SICER and MACS [50]. Overlap between peaks and genomic regions of interest were generated using Perl and Python scripts as well as pybedtools [52, 53]. Figures

Table 1 The list of PCR primers

Unique regions ChIP primers	
pax2-F	CTGGCACTGACATCTTGTTGG
pax2-R	TGGGACCTGTAGTCCTGACC
anapc13-F	TCCTAAGCCGCTCTGTAGTCC
anapc13-R	GGGTGTCCATCATCTGAGTCC
alox8-F	GTATGAGGTGGCCTGAGTG
alox8-R	AAGCCCTGCCTAAATGTGTG
ebf1-F	AACTGAGCCTTAGGGGAAGC
ebf1-R	TCAGGGTTCAATCTCCAAGG
cebpb-F	AGAGTTCTGCTTCCCAGGAGT
cebpb-R	GGAAACAGATCGTTCCTCCA
fez1-F	GAGGGTGGGACGTATTTTCAGT
fez1-R	CAGCCTTCTTCCCTCACAA
pcdhb22-F	GCAAGTAATGCCAGCAATGG
pcdhb22-R	TCCAGTTGGTTGGGTTTCAT
RT-qPCR primers	
Rnh1-F (Housing keeping gene)	TCCAGTGTGAGCAGCTGAG
Rnh1-R (Housing keeping gene)	TGCAGGCACTGAAGCACCA
Nipbl-F	AGTCCATATGCCCCACAGAG
Nipbl-R	ACCGGCAACAATAGGACTTG
Rad21-F	AGCCAAGAGGAAGAGGAAGC
Rad21-R	AGCCAGGTCCAGAGTCGTAA
Cebpb-F	GCGGGGTTGTTGATGTTT
Cebpb-R	ATGCTCGAAACGGAAAAGG
Cebpd-F	ACAGGTGGGAGTGGAGTAA
Cebpd-R	GTGGCACTGTCAACCATACA
Ebf1-F	GCGAGAATCTCCTTCAAGACTTC
Ebf1-R	ACCTACTGCTTTGTGGGTT
Il6-F	TAGTCTTCTACCCCAATTTCC
Il6-R	TTGGTCTTAGCCACTCCTTC
Avpr1a-F	TGGTGGCCGTGCTGGGTAATAG
Avpr1a-R	GCGGAAGCGGTAGGTGATGTC
Lpar1-F	ATTTACAGCCCGATTCCAC
Lpar1-R	CACCAGCTTGCTACTGTGT
Adm-F	TATCAGAGCATCGCCACAGA
Adm-R	TTAGCGCCCACTTATTTCCAC
Cebpb 3C primers	
cebpb-promoter	ACTCCGAATCCTCCATCCTT
cebpb-region-b	CCTGCCCTGTATCAAAGCAT
cebpb-region-a	CTGCCCAAATCAGTGAGGTT
cebpb-region-c	CCTCTGTGAGGTCTGGTCGT
cebpb-promoter-R	GGTGGCTGCGTTAGACAGTA
cebpb-region-a-R	GTTGTATCCCAAGCCAGCTC
cebpb-region-b-R	CTCCCCACTCTGTTCCAGGAC
cebpb-region-c-R	TAACAGCAGGGATGGGTTCT

were generated using the R statistical package [54]. Visualization of sequence pileup utilized the UCSC Genome Browser [55, 56].

Motif analysis

De novo motif discovery was performed using Multiple Expectation maximization for Motif Elicitation (MEME) version 6.1 [57]. Input sequences were limited to 200 bp in length surrounding the summit of any given peak, and the number reduced to 1000 randomly sampled sequences from the set of all peak sequences. Motif searches for known motifs were performed by calculation of a log-odds ratio contrasting the position weight matrix with the background nucleotide frequency. Baseline values were determined from calculations across randomly selected regions of the genome. Randomly selected 200-bp genomic regions were used to calculate a false discovery rate (FDR) at several position weight matrix (PWM) score thresholds. We chose the motif-calling score threshold corresponding to a 4.7% FDR. The p values were derived for the number of matches above the z -score threshold relative to the background using a hypergeometric test.

Expression data analysis

Affymetrix MOE430A 2.0 array data for mouse embryonic fibroblasts (10 data sets for the wild type and nine for Nipbl+/- mutant MEFS) were previously published [19]. Expression data were filtered for probe sets with values below 300 and above 20,000, with the remainder used for downstream analysis. Differential expression and associated p values were determined using Cyber-t, which uses a modified t test statistic [58]. Multiple hypothesis testing correction was performed using a permutation test with 1000 permutations of the sample data. Probe sets were collapsed into genes by taking the median value across all probe sets representing a particular gene. Raw expression values for each gene are represented as a z -score, which denotes the number of standard deviations that value is away from the mean value across all genes. Gene ontology analysis was performed using PANTHER [59, 60] with a cutoff of $p < 0.05$.

KS test

Genes were sorted by their fold-change, and any adjacent ChIP-binding sites were identified. We performed a Kolmogorov-Smirnov (KS) test comparing the expression-sorted ChIP binding presence vs. a uniform distribution of binding sites, similar to Gene Set Enrichment Analysis [61]. If ChIP binding significantly correlates with the gene expression fold-change, the KS statistic, d , will also have significant, non-zero magnitude. To better visualize the KS test, we plotted the difference between the presence of cohesin binding at (expression-sorted) genes in Fig. 5. The

x axis of this figure is the (fold-change-based) gene rank, and the y axis is the KS statistic d , which behaves like a running enrichment score and is higher (lower) when binding sites co-occur more (less) often than expected if there were no correlation between ChIP binding and expression fold-change. The KS test uses only the d with the highest magnitude, which is indicated in the plots by a vertical red line. To better visualize ChIP binding presence, we further plot an x -mirrored density of peak presence at the top of each plot; the gray “beanplot” [62] at the top of the plots are larger when many of the genes have adjacent ChIP-binding sites.

siRNA depletion

Wild type MEFs were transfected using HiPerFect (Qiagen) following the manufacturer’s protocol with 10 mM small interfering RNA (siRNA). A mixture of 30 μ l HiPerFect, 3 μ l of 20 μ M siRNA, and 150 μ l DMEM was incubated for 10 min and added to 2×10^6 cells in 4 ml DMEM. After 6 h, 4 ml fresh DMEM with 10% FBS was added. Transfection was repeated the next day. Cells were harvested 48 h after the first transfection. SiRNAs against *Nipbl* (Nipbl-1: 5’-GTGGTCGTTACCGAAACCGAA-3’; Nipbl-2: 5’-AAGGCAGTACTTAGACTTTAA-3’) and *Rad21* (5’-CTCGAGAATGGTAATTGTATA-3’) were made by Qiagen. AllStars Negative Control siRNA was obtained from Qiagen.

RT-q-PCR

Total RNA was extracted using the Qiagen RNeasy Plus kit. First-strand cDNA synthesis was performed with SuperScript II (Invitrogen). Q-PCR was performed using the iCycler iQ Real-time PCR detection system (Bio-Rad) with iQ SYBR Green Supermix (Bio-Rad). Values were generated based on Ct and normalized to control gene *Rnh1*. PCR primers specific for major satellite, minor satellite, rDNA, and SINE B1 were previously described [48]. Other unique primers are listed in Table 1. The RT-qPCR analyses of the wild type and mutant cells were done with two biological replicates with consistent results. The gene expression changes after siRNA treatment were evaluated with two to three biological replicates with similar results.

3C analysis

The chromosome conformation capture (3C) protocol was performed as described [35]. Approximately 1×10^7 cells were crosslinked with 1% formaldehyde at 37 °C for 10 min. Crosslinking was stopped by adding glycine to a final concentration of 0.125 M. Cells were centrifuged and lysed on ice for 10 min. Nuclei were washed with 500 μ l of 1.2 \times restriction enzyme buffer and resuspended with another 500 μ l of 1.2 \times restriction enzyme buffer with 0.3% SDS and incubated at 37 °C for 1 h.

Triton X-100 was added to 2% and incubated for another 1 h. 800 U of restriction enzyme (HindIII New England Biolabs) was added and incubated overnight at 37 °C. The digestion was heat-inactivated the next day with 1.6% SDS at 65 °C for 25 min. The digested nuclei were added into a 7 ml 1 \times ligation buffer with 1% Triton X-100, followed by 1-h incubation at 37 °C. T4 DNA ligase (2000 U) (New England Biolabs) was added and incubated for 4 h at 16 °C followed by 30 min at room temperature. Proteinase K (300 μ g) was added, and the sample was reverse-crosslinked at 65 °C overnight. Qiagen Gel Purification Kits were used to purify DNA. Approximately 250 ng of template was used for each PCR reaction. PCR products were run on 2% agarose gels with SYBRSafe (Invitrogen), visualized on a Fujifilm LAS-4000 imaging system and quantified using Multi-gauge (Fujifilm).

To calculate interaction frequencies, 3C products were normalized to the constitutive interaction at the excision repair cross-complementing rodent repair deficiency, complementation group 3 (*ercc3*) locus [63, 64], which is unaffected in mutant MEFs. A control template was made to control for primer efficiencies locus-wide as described [65]. PCR fragments spanning the restriction sites examined were gel purified, and equimolar amounts were mixed (roughly 15 μ g total) and digested with 600 U restriction enzyme overnight and subsequently ligated at a high DNA concentration (> 300 ng/ μ l). The template was purified with the Qiagen PCR Purification Kit and mixed with an equal amount of digested and ligated genomic DNA. Two hundred fifty nanograms of the resulting control template was used for each PCR for normalization against PCR primer efficiencies. Two biological replicates with three technical replicates each were analyzed for both wild type and mutant cells and for control and *Nipbl* siRNA-treated cells, which yielded consistent results.

Results

Nipbl haploinsufficiency leads to a global reduction of cohesin binding to its binding sites

In order to investigate how *Nipbl* haploinsufficiency leads to CdLS, cohesin binding was examined genome-wide by ChIP-seq analyses using antibody specific for the cohesin subunit *Rad21*, in wild type and *Nipbl*^{+/-} mutant MEFs derived from E15.5 embryos [19] (Fig. 1a). MEFs derived from five wild type and five mutant pups from two litters were combined to obtain sufficient chromatin samples for ChIP-seq analysis. *Nipbl*^{+/-} mutant MEFs express approximately 30–40% less *Nipbl* compared to wild type MEFs [19] (Table 2). MEFs from this embryonic stage were chosen in order to match with a previous expression microarray study, because they are relatively

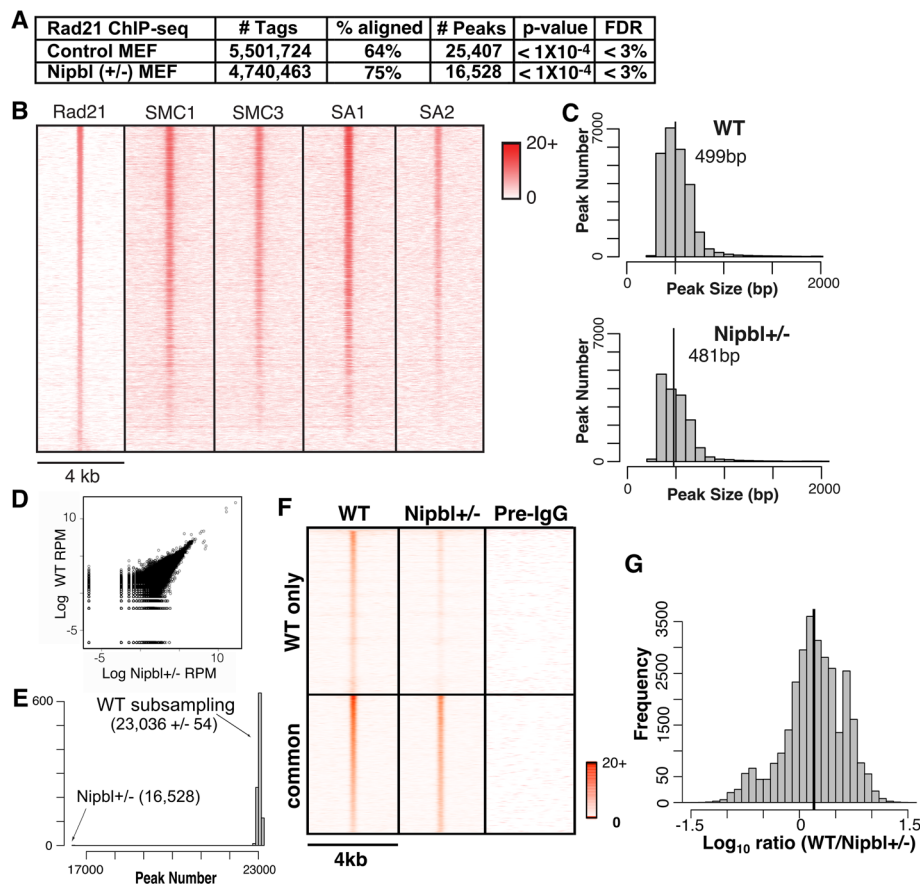


Fig. 1 Global decrease of cohesin binding to chromatin in *Nipbl* heterozygous mutant MEFs. **a** Cohesin-binding sites identified by ChIP-sequencing using antibody specific for Rad21 in control wild type and *Nipbl*^{+/-} MEFs. Peak calling was done using AREM [50]. The *p* value and FDR are shown. **b** Heatmap comparison of Rad21 ChIP-seq data with those of SMC1, SMC3, SA1, and SA2. Rad21 peaks in the wild type MEFs are ranked by strongest to weakest and compared to the ChIP-seq data of SMC1, SMC3, SA1, and SA2 in MEFs (GSE32320) [67] in the corresponding regions. The normalized (reads per million) tag densities in a 4-kb window around each Rad21 peak are plotted, with peaks sorted from the highest number of tags in the wild type MEFs to the lowest. **c** Histogram of cohesin peak widths in wild type and mutant MEFs, indicating the number of peaks in a given size range. The segmentation of the histogram is at 100 bp intervals. The median value is indicated with a vertical black line and labeled. **d** Scatter plot of histone H3 ChIP-seq tag counts in wild type and mutant MEFs in 500 bp bins across the mouse genome. The values are plotted in log reads per million (RPM). **e** Histogram showing the distribution of total peaks called. A comparable number of reads to the *Nipbl*^{+/-} mutant dataset (i.e., 4,740,463) were sub-sampled from the wild type dataset, and peaks called using only the sub-sampled reads. This process was performed 1000 times to produce the histogram above. Mean values with standard deviations are shown. **f** Heatmap analysis of cohesin binding in wild type (WT) MEFs and corresponding peak signals in *Nipbl*^{+/-} MEFs. The normalized (reads per million) tag densities in a 4-kb window around each peak are plotted, with peaks sorted from the highest number of tags in the wild type to the lowest. Peaks are separated into two categories, those that are found only in wild type ("WT only") and those that overlap between wild type and *Nipbl*^{+/-} ("common"). Preimmune IgG ChIP-seq signals in the corresponding regions are also shown as a control. The color scale indicates the number of tags in a given region. **g** Histogram of the ratio between normalized (reads per million total reads) wild type and mutant reads in peaks common to both. Positive values indicate more wild type tags. The black line indicates the mean ratio between wild type and mutant tag counts

free of secondary effects caused by *Nipbl* mutation-induced developmental abnormalities compared to embryonic tissue [19]. Consistent with this, there is no noticeable difference in growth rate and cell morphology between normal and mutant MEFs [19]. This particular anti-Rad21 antibody was used previously for ChIP analysis and was shown to identify holo-cohesin complex binding sites [30, 35, 45, 66]. This is consistent with the close correlation of the

Table 2 *Nipbl* and Rad21 depletion levels in mutant and siRNA-treated MEFs

Gene	<i>Nipbl</i> ^{+/-} mutant	<i>Nipbl</i> siRNA	Rad21 siRNA
<i>Nipbl</i>	0.68 ± 0.003	0.68 ± 0.001	1.04 ± 0.051
Rad21	0.94 ± 0.021	0.99 ± 0.021	0.26 ± 0.018
CTCF	0.95 ± 0.050	0.96 ± 0.066	0.84 ± 0.074

presence of other cohesin subunits at identified Rad21-binding sites [67] (Fig. 1b).

Cohesin-binding sites were identified using AREM [50], with a significance cutoff based on a p value less than 1×10^{-4} , resulting in a FDR below 3.0% (Fig. 1a). Cohesin-binding peaks ranged from ~ 200 bp to ~ 6 kb in size with the majority less than 1 kb in both wild type and mutant cells (median value of 499 bp in wild type and 481 bp in mutant cells) (Fig. 1c). Approximately 35% fewer cohesin-binding sites were found in *Nipbl*^{+/-} mutant MEFs compared to the wild type MEFs (Fig. 1a). This is not due to variability in sample preparation since no significant difference in the histone H3 ChIP-seq was observed between the wild type and mutant cell samples (R value = 0.96) (Fig. 1d). Since the total read number for mutant ChIP-seq was $\sim 15\%$ less than for wild type ChIP-seq (Fig. 1a), we examined whether the difference was in part due to a difference in the number of total read sequences between the two Rad21 ChIP samples. To address this, we randomly removed reads from the wild type sample to match the number of reads in the mutant sample and ran the peak discovery algorithm again on the reduced wild type read set. This was repeated 1000 times. We found that the wild type sample still yielded $\sim 39\%$ more peaks than the mutant, indicating that identification of more peaks in the wild type sample is not due to a difference in the numbers of total read sequences (Fig. 1e). Thus, cohesin appears to bind to fewer binding sites in *Nipbl* haploinsufficient cells.

The above results might suggest that a significant number of binding sites are unique to the wild type cells (Fig. 1a). When we compared the raw number of reads located within wild type peaks and the corresponding regions in mutant MEFs, however, we noted a reduced, rather than a complete absence of, cohesin binding in mutant cells (Fig. 1f). Those regions in mutant cells corresponding to the “WT only” regions consistently contain one to three tags in a given window, which are below the peak cutoff. However, the signals are significant compared to the negative control of preimmune IgG (Fig. 1f). Furthermore, even for those sites that are apparently common between the control and mutant MEFs, the binding signals appear to be weaker in mutant cells (Fig. 1f). To validate this observation, we segmented the genome into nonoverlapping 100 bp bins and plotted a histogram of the log ratios of read counts between the wild type and mutant samples in each bin, with read counts normalized using reads per kilobase per million total reads (RPKM) [68]. The plot indicates that the read counts for the mutant bins are generally less than those for the wild type bins, even for the binding sites common to both wild type and mutant cells (Fig. 1g). Signal intensity profiles of the Rad21 ChIP-seq in the selected gene regions also show a general decrease

of Rad21 binding at its binding sites in *Nipbl*^{+/-} MEFs compared to the control MEFs (see Fig. 6b). Decreased cohesin binding was further confirmed by manual ChIP-qPCR analysis of individual cohesin-binding sites using at least three independent control and mutant MEF samples supporting the reproducibility of the results (see Fig. 3). Decreased cohesin binding was also observed at additional specific genomic regions in *Nipbl*^{+/-} MEFs [69]. Taken together, the results indicate that cohesin binding is generally decreased at its binding sites found in wild type MEFs, rather than re-distributed, in mutant MEFs.

The relationship of cohesin-binding sites with CTCF-binding sites and CTCF motifs

It has been reported that cohesin binding significantly overlaps with CTCF sites and depends on CTCF [30, 31]. A study in mouse embryonic stem cells (mESCs) showed, however, that there is only a limited overlap between CTCF- and *Nipbl*-bound cohesin sites, suggesting that there are two categories of cohesin-binding sites and the latter may be particularly important for gene activation [40]. Other studies also revealed that ~ 20 – 30% of cohesin sites in different human cancer cell lines and up to $\sim 50\%$ of cohesin sites in mouse liver appear to be CTCF-free [42, 43]. Some of these non-CTCF sites overlap with sequence-specific transcription factor binding sites in a cell type-specific manner, highlighting the apparent significance of CTCF-free cohesin sites in cell type-specific gene expression [42, 43]. De novo motif discovery by MEME identified the CTCF motif to be the only significant motif associated with cohesin-binding sites in our MEFs (Fig. 2a). Comparing our cohesin peaks with experimentally determined CTCF-binding peaks in MEFs [40], we found that approximately two thirds of cohesin-binding sites detected by Rad21 ChIP overlapped CTCF-binding sites (Fig. 2b). This is comparable with what was initially observed in mouse lymphocytes [30] and HeLa cells [31] using antibodies against multiple cohesin subunits. In contrast to recent studies reporting that almost all the CTCF-binding sites overlap with cohesin [43], our results show that less than 60% of CTCF-binding sites are co-occupied with cohesin (Fig. 2b). This is consistent with the fact that CTCF binds and functions independently of cohesin at certain genomic regions [34, 41, 70, 71].

The presence of a CTCF motif closely correlates with CTCF binding: over 90% of cohesin-binding sites overlapping with CTCF peaks contain CTCF motifs (Fig. 2c). In contrast, less than half of cohesin-binding sites harbor CTCF motifs in the absence of CTCF binding. Cohesin-binding sites without CTCF binding tend to be highly deviated from a CTCF motif, reflecting a CTCF-independent mechanism of recruitment (Fig. 2d). Interestingly, a small population of cohesin-CTCF overlapped

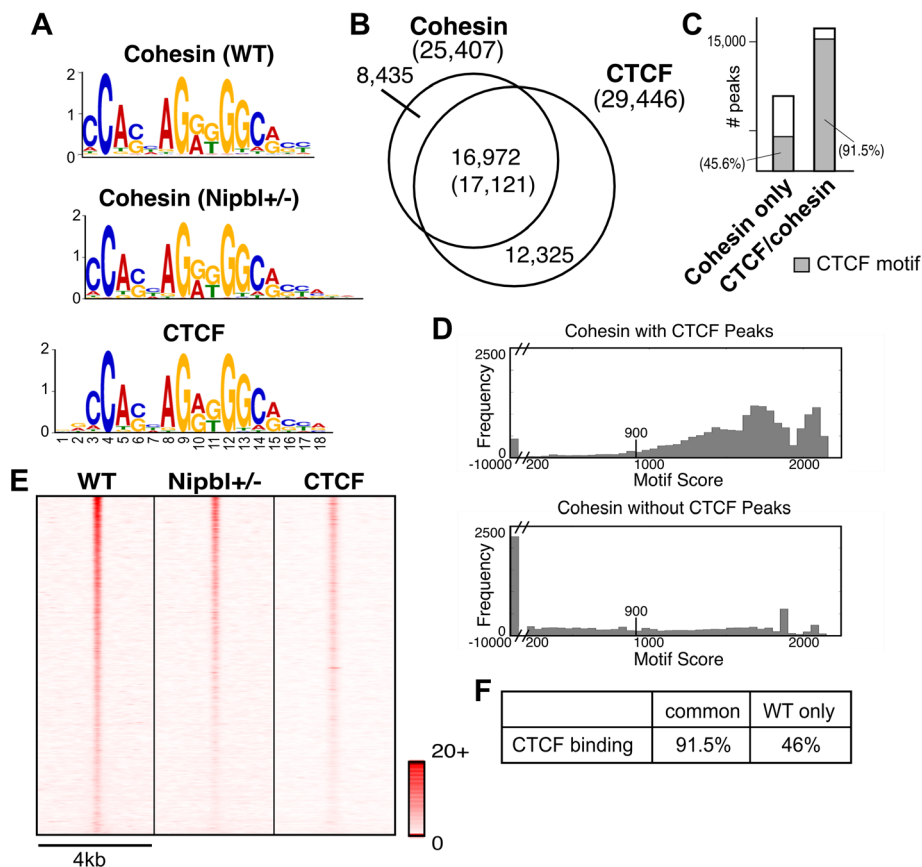


Fig. 2 Most of cohesin-binding sites contain CTCF motifs. **a** De novo motif search of cohesin-binding sites using MEME. The CTCF motifs identified at the cohesin-binding sites in WT and mutant MEFs are compared to the CTCF motif obtained from CTCF ChIP-seq data in MEFs (GSE22562) [40]. *E* values are 5.5e–1528 (cohesin-binding sites in WT MEFs), 6.6e–1493 (cohesin-binding sites in Nipbl MEFs), and 2.6e–1946 (CTCF-binding sites in MEFs), respectively. **b** Overlap of cohesin binding sites with CTCF binding sites. The number in the parenthesis in overlapping regions between cohesin and CTCF binding represents the number of CTCF-binding peaks. **c** Presence of CTCF motifs in cohesin only and cohesin/CTCF-binding sites. Shaded area represents binding sites containing CTCF motifs defined in **a** (FDR 4.7%). **d** The CTCF motif score distribution for all cohesin peaks that overlap with a CTCF peak (top) and that do not overlap with a CTCF peak (bottom). Note that the *X* axis is discontinuous and scores less than 200 are placed in the single bin in each figure. For peaks that contained multiple CTCF motifs, we report the maximum score for the peak. The score threshold (900 with FDR 4.7%) is marked in each figure. **e** Heatmap comparison of cohesin ChIP-seq tags in WT MEFs and Nipbl mutant MEFs with CTCF ChIP-seq tags at the corresponding regions in wild type MEFs [40] as indicated at the top. The normalized (reads per million total reads) tag densities in a 4-kb window (± 2 kb around the center of all the cohesin peaks) are plotted, with peaks sorted by the number of cohesin tags (highest at the top) in WT MEFs. Tag density scale from 0 to 20 is shown. **f** Percentages of CTCF binding in cohesin-binding sites common or unique to WT MEFs

sites also lack any CTCF motif, suggesting an alternative way by which cohesin and CTCF bind to these regions (Fig. 2c, d).

Nipbl reduction affects cohesin binding at CTCF-bound sites and repeat regions

In mESCs, it was proposed that Nipbl and CTCF recruit cohesin to different genomic regions, implying that cohesin binding to CTCF sites may be Nipbl-independent [40]. We noticed that when we ranked cohesin-binding sites based on the read number in wild type peaks, they matched closely with the ranking of cohesin-binding sites in mutant MEFs, indicating that the decrease of cohesin binding is roughly proportional to the strength of the original binding signals (Fig. 2e).

This suggests that most cohesin-binding sites have similar sensitivity to Nipbl reduction. Importantly, CTCF-binding signals also correlate with the ranking of cohesin binding, indicating that CTCF-bound sites are in general better binding sites for cohesin (Fig. 2e). Because of this, they satisfy the peak definition despite the decrease of cohesin binding in mutant cells (Fig. 1f, g and Fig. 6b). This explains why CTCF-bound cohesin sites are apparently enriched in the sites that are common to both wild type and mutant cells (Fig. 2f).

Based on the above data, we further clarified the role of Nipbl in cohesin binding to CTCF sites. We compared the effect of Nipbl reduction on cohesin binding to representative sites, which have either CTCF binding or a CTCF motif or both (Fig. 3a). Decreased cohesin

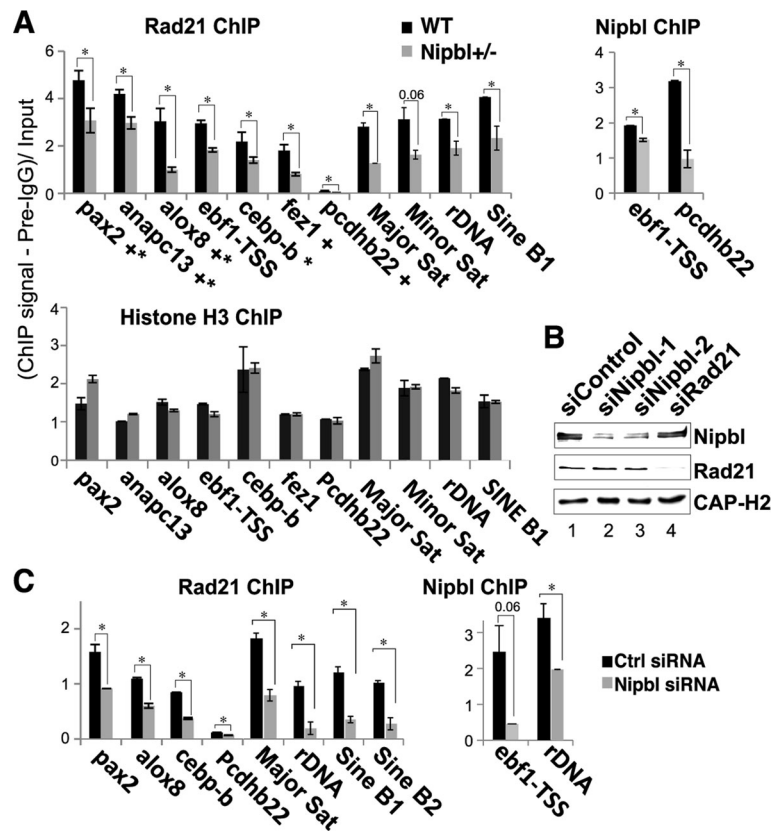


Fig. 3 Nipbl reduction decreases cohesin binding. **a** Manual ChIP-q-PCR of cohesin-binding sites at unique gene regions and repeat regions using anti-Rad21 antibody (top left) compared to histone H3 (bottom) in Nipbl+/- mutant and wild type MEFs. Representative examples of Nipbl ChIP are also shown (top, right). "Plus sign" indicates CTCF binding, and "asterisk" indicates the presence of motif. PCR signals were normalized with preimmune IgG (pre-IgG) and input. * $p < 0.05$. **b** Western blot analysis of control, Nipbl, or Rad21 siRNA-treated cells is shown using antibodies indicated. Depletion efficiency and specificity of Nipbl siRNA were also examined by RT-q-PCR (Table 2). Nipbl protein depletion was estimated to be ~80% (siNipbl-1) and 60% (siNipbl-2) according to densitometric measurement (lanes 2 and 3, respectively). Comparable ChIP results were obtained by the two Nipbl siRNAs (data not shown). **c** Similar manual ChIP-q-PCR analysis as in **a** in control and Nipbl siRNA (siNipbl-1)-treated MEFs

binding was observed at sites tested by manual ChIP-qPCR in Nipbl mutant MEFs, correlating with the decreased Nipbl binding (Fig. 3a). Consistent with the genome-wide ChIP-seq analysis (Fig. 1a), control histone H3 ChIP-qPCR revealed no significant differences at the corresponding regions, indicating that the decreased cohesin binding is not due to generally decreased ChIP efficiency in mutant MEFs compared to the wild type MEFs (Fig. 3a, bottom). Similar results were obtained using a small interfering RNA (siRNA) specific for *Nipbl* (Fig. 3c), which reduced Nipbl to a comparable level as in mutant cells (western blot in Fig. 3b and RT-qPCR results in Table 2). This demonstrates the specificity of the Nipbl antibody and confirms that the decreased cohesin binding seen in Nipbl mutant MEFs is the consequence of reduced Nipbl (Fig. 3a). Thus, Nipbl also functions in cohesin loading at CTCF sites.

Repeat sequences are often excluded from ChIP-seq analysis. However, cohesin binding is found at various repeat sequences, including pericentromeric and subtelomeric

heterochromatin, and ribosomal DNA regions in the context of heterochromatin in mammalian cells [44, 45]. Thus, we also tested the effect of Nipbl reduction on cohesin binding to repeat sequences by manual ChIP-PCR (Fig. 3). Both *Nipbl* mutation (Fig. 3a, top) and Nipbl depletion by siRNA (Fig. 3b, c) resulted in decreased cohesin binding at the repeat regions, indicating that Nipbl is also important for cohesin binding to repeat sequences. In contrast, there were no significant differences in the histone H3 ChIP signals between these repeat regions in wild type and mutant MEFs (Fig. 3a, bottom). Taken together, the results indicate that Nipbl functions in cohesin loading even at CTCF sites and repeat regions, confirming the genome-wide decrease of cohesin binding caused by Nipbl haploinsufficiency.

Cohesin distribution patterns in the genome and enrichment in promoter regions

In order to gain insight into how the weakening of cohesin binding may affect gene expression in mutant cells,

the distribution of cohesin-binding sites in the genomes of both wild type and mutant MEFs were examined. Approximately, 50% of all cohesin-binding sites are located in intergenic regions away from any known genes (Fig. 4a). However, there is a significant enrichment of cohesin binding in promoter regions, and to a lesser extent in the 3' downstream regions, relative to the random genomic distribution generated by sampling from pre-immune ChIP-seq reads (Fig. 4b). Similar promoter and downstream enrichment has been observed in mouse and human cells [30, 31, 40, 42, 67] as well as in *Drosophila* [72]. Promoter enrichment is comparable in both wild type and *Nipbl* mutant MEFs, constituting ~10% of all the cohesin-binding sites (Fig. 4a). Thus, there is no significant redistribution or genomic region-biased loss of cohesin-binding sites in *Nipbl* mutant cells.

Cohesin-bound genes are sensitive to *Nipbl* haploinsufficiency

Based on the significant enrichment of cohesin binding in the promoter regions, we next examined the correlation between cohesin binding to the gene regions and the change of gene expression in mutant MEFs using a KS test. This is a nonparametric test for comparing peak binding sites with gene expression changes in the mutant MEFs (Fig. 5). Genes that displayed the greatest expression change in mutant MEFs compared to the wild type MEFs showed a strong correlation with cohesin binding to the gene region, indicating that direct binding to the target genes is the major mechanism by which cohesin mediates gene regulation in a *Nipbl* dosage-sensitive fashion (Fig. 5a, left). Random sampling of a comparable number of simulated peaks in the gene regions yielded no correlation (Fig. 5d, left). Interestingly, cohesin binding to the gene region correlates better with decreased gene expression than increased expression in

mutant cells, indicating that gene activation, rather than repression, is the major mode of cohesin function at the gene regions (Fig. 5a, middle).

When analyzed separately, cohesin binding to the promoter regions (+2.5 kb to -0.5 kb of transcription start sites (TSS) (Fig. 5a, right)) showed the highest correlation (p value = $3.3e-09$) compared to the gene body and downstream (Fig. 5b). Thus, cohesin binding to the promoter regions is most critical for gene regulation. Similar to the entire gene region, cohesin binding correlates more significantly with a decrease in gene expression in mutant cells, which is particularly prominent at the promoter regions compared to gene bodies or downstream, indicating the significance of cohesin binding to the promoter regions in gene activation (Fig. 5c). Cohesin and CTCF binding closely overlapped at promoter regions in HeLa cells [31]. However, the overlap of CTCF binding with cohesin in MEFs is lower in the promoter regions (54%) than that in the intergenic regions (67%) [40]. Consistent with this, there is no significant correlation between CTCF binding in the promoter regions and gene expression changes in *Nipbl* mutant MEFs (p value = 0.28) by KS test (Fig. 5c, right). These results further indicate the cohesin-independent and *Nipbl*-insensitive function of CTCF in gene regulation. Taken together, the results suggest that cohesin binding to gene regions (in particular, to promoters) is significantly associated with gene activation that is sensitive to *Nipbl* haploinsufficiency.

Identification of cohesin target genes sensitive to *Nipbl* haploinsufficiency

The results above indicate that cohesin-bound genes sensitive to a partial loss of *Nipbl* can be considered to be *Nipbl*/cohesin target genes. Among 218 genes that changed expression significantly in mutant cells

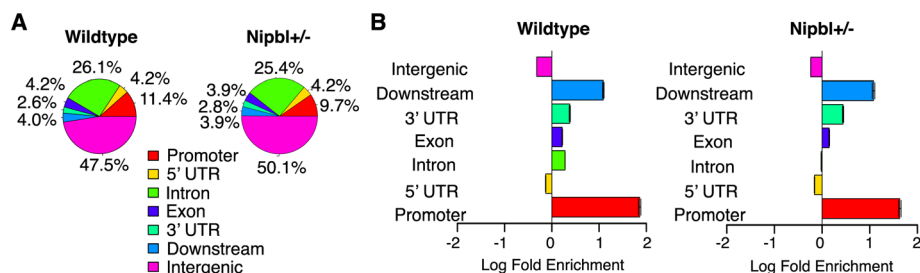


Fig. 4 Cohesin-binding site distribution in the genome in MEFs. **a** Percentage distribution of cohesin peaks in genomic regions. “Promoter” and “Downstream” is defined as 2500 bp upstream of the transcription start site (TSS) and 500 bp downstream of the TSS, and “Downstream” represents 500 bp upstream of transcription termination site (TTS) and 2500 bp downstream of TTS. The 3' and 5' untranslated regions (UTRs) are defined as those annotated by the UCSC genome browser minus the 500 bp interior at either the TSS or TTS. When a peak overlaps with multiple regions, it is assigned to one region with the order of precedence of promoter, 5' UTR, Intron, Exon, 3'UTR, downstream, and intergenic. **b** Enrichment of cohesin peaks across genomic regions as compared to randomly sampled genomic sequence. A comparable number of peaks (25,407 and 16,528 peaks in wild type and mutant MEFs, respectively), with the same length as the input set, were randomly chosen 1000 times and the average used as a baseline to determine enrichment in each genomic region category

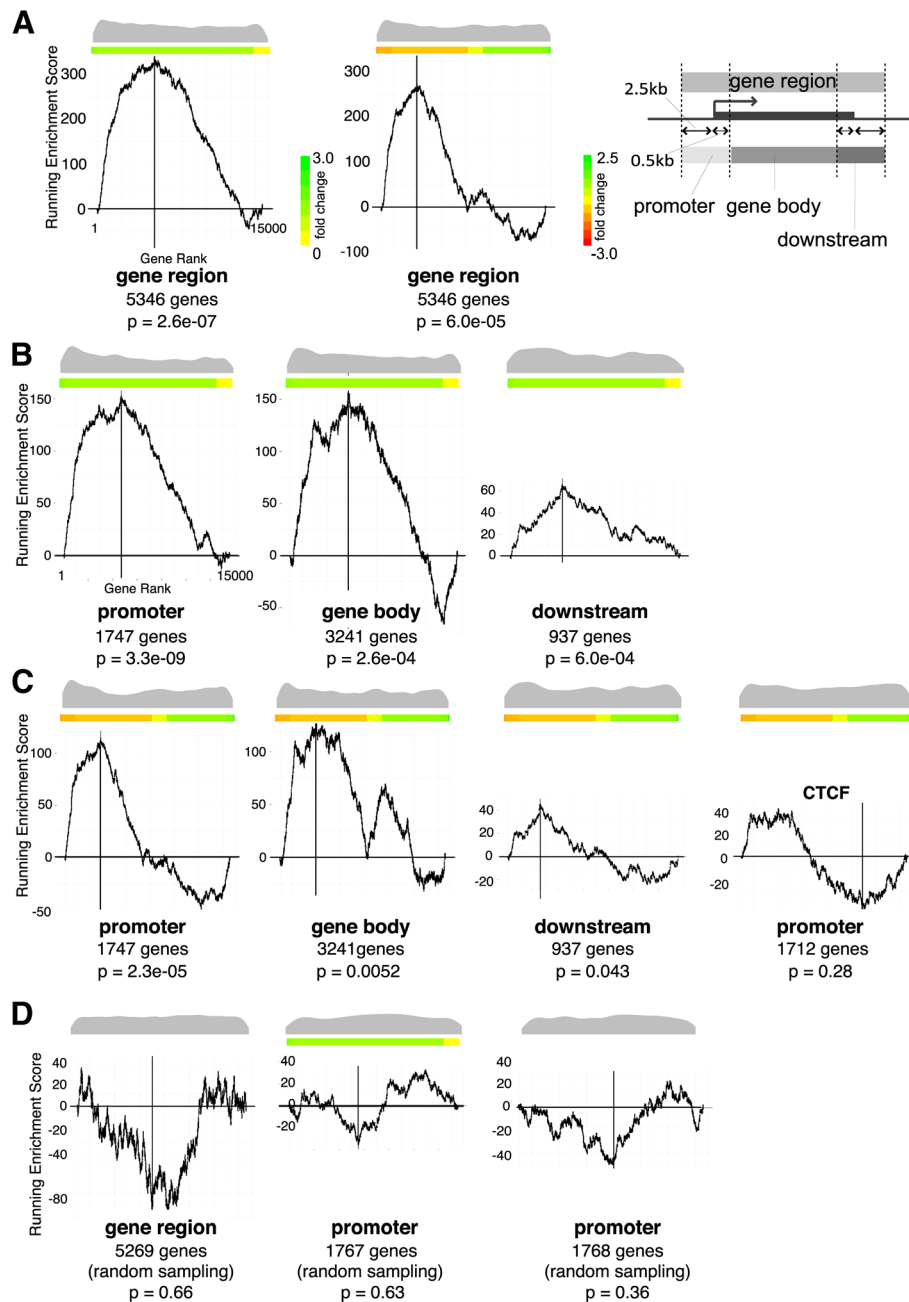


Fig. 5 Correlation of cohesin binding and gene expression changes in mutant MEFs. **a** KS test indicating the degree of cohesin binding to genes changing expression in *Nipbl*^{+/-} MEFs. X-axis represents all 13,587 genes from the microarray data [19] ranked by absolute fold expression changes from biggest on the left to the smallest on the right in the left panel. Fold changes are shown in different colors as indicated on the side. In the middle panel, gene expression changes were ranked from negative to positive with the color scale shown on the side. Both color scales apply to the rest of the figure. The Y-axis is the running enrichment score for cohesin binding (see the "Methods" section for details). Distribution of cohesin-bound genes among 13,587 genes examined is shown as a beanplot [62] at the top, and the number of cohesin-bound genes and p values are shown underneath. The schematic diagram showing the definition of the gene regions, promoter (2.5 kb upstream and 0.5 kb downstream of TSS), gene body, and downstream (2.5 kb downstream and 0.5 kb upstream of TTS) regions is shown on the right. **b** Similar KS test analysis as in **a**, in which cohesin binding to the promoter, gene body, and downstream regions are analyzed separately. **c** Genes are ranked by expression changes from positive on the left to negative on the right. Fold changes are shown by different colors as indicated on the right. CTCF binding to promoter regions (GSE22562) [40] was analyzed for a comparison. **d** Lack of correlation between the mutant expression changes and randomly chosen genes are shown on the right as a negative control

compared to the wild type (> 1.2 -fold change, p value < 0.05) [19], we found that more than half (115 genes) were bound by cohesin and thus can be considered *Nipbl*/cohesin target genes (Table 3). This is a conservative estimate of the number of direct target genes since cohesin-binding sites beyond the upstream and downstream cutoffs (2.5 kb) were not considered for the analysis. Consistent with the KS test analysis (Fig. 5), $\sim 74\%$ of these cohesin target genes were downregulated in mutant cells, indicating that the positive effect of cohesin on gene expression is particularly sensitive to partial reduction of *Nipbl* (Table 3).

Many of these *Nipbl*/cohesin-target genes contain cohesin-binding sites in more than one region (promoter, gene body and/or downstream), suggesting their collaborative effects (Fig. 6a). In particular, the promoter binding of cohesin is often accompanied by its binding to the gene body. However, binding pattern analysis revealed no significant correlation between a particular pattern and/or number of cohesin-binding sites and gene activation or repression (Fig. 6a). Rad21 ChIP-seq signal intensity profiles of several cohesin target genes (as defined above) reveal decreased cohesin binding in mutant cells at the binding sites originally observed in the wild type cells, supporting the notion that gene expression changes are the direct consequence of the reduced cohesin binding (Fig. 3a; Fig. 6b, top). There are other genes, however, that did not change expression significantly in mutant MEFs, but nevertheless also have reduced cohesin peaks nearby (Fig. 6b, bottom), suggesting that cohesin binding is not the sole determinant of the gene's expression status and that its effect is context-dependent.

Gene ontology analysis revealed that the target genes bound by cohesin at the promoter regions and affected by *Nipbl* deficiency are most significantly enriched for those involved in development (Table 4). The results suggest a direct link between diminished *Nipbl*/cohesin and the dysregulation of developmental genes, which contributes to the CdLS phenotype.

***Nipbl*- and cohesin-mediated activation of adipogenesis genes**

One of the reported phenotypes of *Nipbl*^{+/-} mice is their substantial reduction of body fat that mirrors what

is observed in CdLS patients [19, 73]. It was found that *Nipbl*^{+/-} MEFs exhibit dysregulated expression of several genes involved in adipocyte differentiation and reduced spontaneous adipocyte differentiation in vitro [19, 73]. We therefore examined the effect of *Nipbl* haploinsufficiency on these adipogenesis genes in detail. We found that many of them are bound by cohesin, in some cases at multiple sites, suggesting that cohesin plays a direct role in activation of these genes (Fig. 7). Although *Il6* and *Cebpd* were originally not included in the 115 genes due to low p values in the microarray analysis (Table 3 and Fig. 6a), significant expression changes were observed in mutant MEFs compared to the wild type MEFs by manual RT-qPCR. *TNF α* and *PPAR γ* , also involved in adipogenesis, do not change their expression in mutant MEFs [19]. Importantly, a decrease of gene expression was observed not only in *Nipbl*^{+/-} mutant cells but also by siRNA depletion of *Nipbl*, confirming that the effect is specifically caused by *Nipbl* reduction (Fig. 7a). Furthermore, depletion of cohesin itself decreased their expression even more significantly than *Nipbl* depletion. The results suggest that multiple genes involved in the adipogenesis pathway are direct cohesin targets that are sensitive to *Nipbl* haploinsufficiency.

Cohesin binding correlates significantly with H3K4me3 at the promoter

To investigate the genomic features associated with cohesin target genes, we examined the chromatin status of the target gene promoters. We found that cohesin peaks closely overlap with the peaks of H3K4me3, a hallmark of an active promoter, in a promoter-specific manner (Fig. 8a). In contrast, there are only minor peaks of H3K27me3 and even less H3K9me3 signal at cohesin-bound promoters. This is consistent with the results of the KS-test revealing the significant association of cohesin binding to the promoter regions with gene activation rather than repression (Fig. 5c). Interestingly, however, promoter binding of cohesin was found in genes with different expression levels in wild type MEFs, revealing no particular correlation with high gene expression (Fig. 8b). Cohesin target genes defined above (Table 3) also exhibit variable expression levels in wild type MEFs (Fig. 8b). Thus, their expression is altered in *Nipbl* mutant cells regardless of the original expression level in wild

Table 3 Gene expression changes and cohesin-binding status

	Total	Cohesin binding				
		Gene region	Promoter	Gene body	Downstream	None
Total	218	115	61	83	20	103
Upregulated	62	30	14	22	6	32
Downregulated	156	85	47	61	14	71

(Fold change > 1.2 ; p value < 0.05)

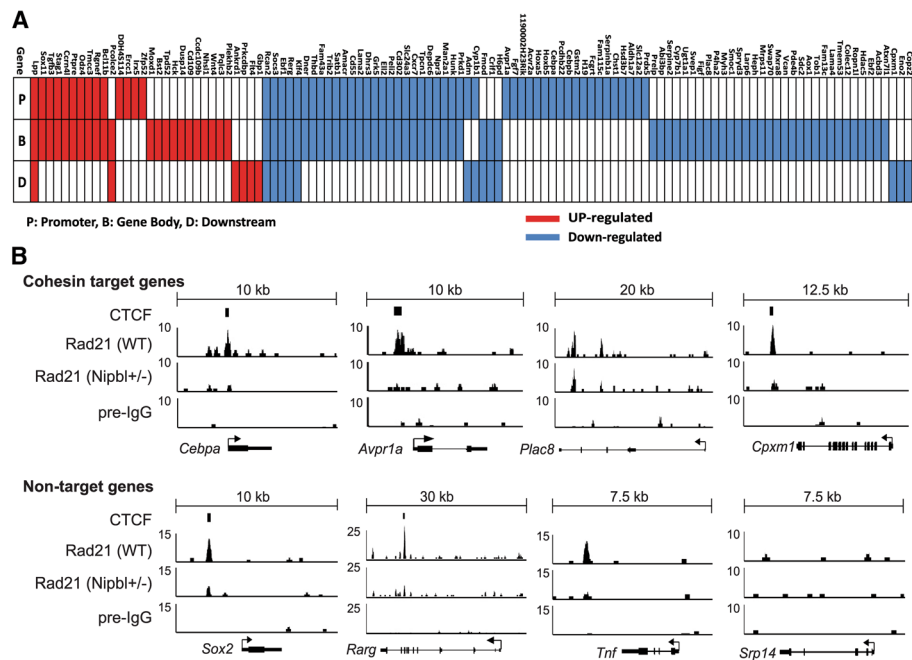


Fig. 6 Cohesin-binding signals at specific gene regions. **a** Cohesin-binding site distribution in cohesin target genes as defined in Table 1. Cohesin binding to the promoter (P), gene body (B), and/or downstream region (D) are indicated for each cohesin target gene in red (upregulated) and blue (downregulated) boxes. **b** Signal intensity profiles of Rad21 ChIP-seq at specific gene regions in wild type and Nipbl mutant MEFs. Preimmune IgG ChIP-seq signals are shown as a negative control. Experimentally determined CTCF-binding peaks in MEFs [40] are also indicated. Examples of genes that are bound by cohesin and changed expression in Nipbl^{+/-} MEFs (top) and those genes that did not change expression (bottom) are shown. No cohesin-binding peaks were found at the *Srp14* gene region

type cells, indicating that cohesin binding contributes to gene expression but does not determine the level of transcription per se.

When cohesin-bound genes were categorized in five different groups based on the gene expression status in wild type MEFs, significant H3K4me3 enrichment was observed even in the cohesin-bound promoters of genes with low expression, compared to cohesin-free promoters of genes with a similar expression level (Fig. 8c). Bivalent (H3K4me3 and H3K27me3) modifications are also enriched in the lowest gene expression category (Fig. 8c). Taken together, the results reveal that there is a close correlation between cohesin binding and H3K4me3 in the promoter regions regardless of the expression levels of the corresponding genes.

Reduced cohesin binding due to NIPBL reduction can lead to a loss of long-distance chromatin interaction

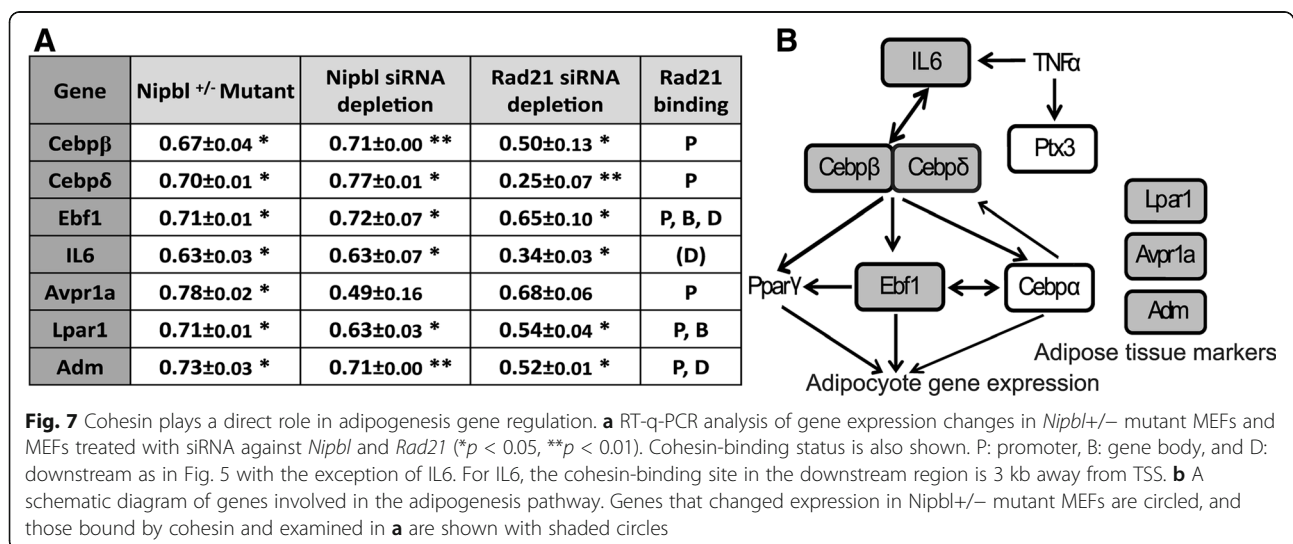
The above results revealed the critical association of cohesin binding to the promoter region and expression of the target genes. How does cohesin bound to the promoter affect gene expression? We recently showed that cohesin-mediated long-distance chromatin interaction between distal enhancer and promoter regions was reduced at the β -globin locus, resulting in reduced gene expression, in Nipbl mutant mice [35].

Thus, we tested the potential involvement of cohesin binding to the *Cebpb* gene, one of the target adipogenesis genes described above, in such long-distance chromatin interaction(s) and whether it is affected by Nipbl reduction using chromosome conformation capture (3C) analysis (Fig. 9). We tested several flanking sites that are positive for cohesin and RNA polymerase II (pol II) binding as well as H3K4me1 and H3K4me3, the hallmarks for enhancers [74–76] (Fig. 9A). We observed that the *Cebpb* promoter interacts with one such region (Fig. 9A, B, the site “c”). Although the site c is associated with only a weak Rad21 ChIP-seq signal, SMC1 and SMC3 ChIP-seq signals were found at the same region [67], confirming that this is an authentic cohesin-binding site (Fig. 9A). The results indicate a selectivity of chromatin interactions among neighboring cohesin-binding sites, revealing that not all proximal cohesin-binding sites interact with each other. Since the other two regions are also bound by CTCF, this may be due to the directionality of CTCF/cohesin binding [77, 78]. Importantly, the observed interaction is indeed reduced in both Nipbl mutant and Nipbl siRNA-treated MEFs (Fig. 9B). The 3C signals at the *Cebpb* locus were normalized to the constant interaction observed at the *Erc3* locus [63, 64], which was not affected by

Table 4 Ontology analysis of cohesin target genes

Biological process	P value	Enrichment	Gene number	Expected number	Genes
Altered gene expression in <i>Nipbl</i> +/- MEFs associated with cohesin binding to the promoters					
Development	2.96E-04	2.38	18	7.55	<i>Avpr1a</i> , <i>Dner</i> , <i>Fgf7</i> , <i>Thbd</i> , <i>Hoxa5</i> , <i>Hoxb5</i> , <i>Cebpa</i> , <i>Cebpb</i> , <i>Rcan2</i> , <i>Lama2</i> , <i>Ebf1</i> , <i>Klf4</i> , <i>Hunk</i> , <i>Tgfb3</i> , <i>Irx5</i> , <i>Odz4</i> , <i>Ptpre</i> , <i>Lpp</i>
Metabolism	2.90E-03	1.50	33	22	<i>Dner</i> , <i>Acvr2a</i> , <i>Hoxa5</i> , <i>Hoxb5</i> , <i>Trib2</i> , <i>Satb1</i> , <i>Cebpa</i> , <i>Cebpb</i> , <i>Gstm2</i> , <i>Amacr</i> , <i>Cd55</i> , <i>Dhrs3</i> , <i>Grk5</i> , <i>Ell2</i> , <i>Serpib1a</i> , <i>Cyp1b1</i> , <i>Chst1</i> , <i>Hsd3b7</i> , <i>Aldh1a7</i> , <i>Npr3</i> , <i>Man2a1</i> , <i>Klf4</i> , <i>Hunk</i> , <i>Prkd1</i> , <i>Prdx5</i> , <i>Erc1</i> , <i>Irx5</i> , <i>Odz4</i> , <i>Sox11</i> , <i>Ptpre</i> , <i>Ccrn4</i> , <i>Rgnef</i> , <i>Bcl11b</i>
Cell communication	2.96E-03	1.82	21	11.53	<i>Dner</i> , <i>Acvr2a</i> , <i>Trib2</i> , <i>Cd55</i> , <i>Grk5</i> , <i>Hunk</i> , <i>Odz4</i> , <i>Ptpre</i> , <i>Rgnef</i> , <i>Avpr1a</i> , <i>Fgf7</i> , <i>Thbd</i> , <i>Fam43a</i> , <i>Rcan2</i> , <i>Socs3</i> , <i>Lama2</i> , <i>Cxcr7</i> , <i>Tpcn1</i> , <i>Rerg</i> , <i>Tgfb3</i> , <i>Lpp</i>
Immune system	6.44E-03	2.06	14	6.81	<i>Dner</i> , <i>Cd55</i> , <i>Hunk</i> , <i>Ptpre</i> , <i>Thbd</i> , <i>Lama2</i> , <i>Cxcr7</i> , <i>Cebpa</i> , <i>Cebpb</i> , <i>Gstm2</i> , <i>Klf4</i> , <i>Prdx5</i> , <i>Fcgrt</i> , <i>Cd302</i>
Altered gene expression in <i>Nipbl</i> +/- MEFs associated with cohesin binding to the gene regions					
Immune system	6.60E-06	2.34	30	12.83	<i>Klf4</i> , <i>Dner</i> , <i>Thbd</i> , <i>Cd55</i> , <i>Lama2</i> , <i>Cd302</i> , <i>Cxcr7</i> , <i>Hunk</i> , <i>Cebpa</i> , <i>Cebpb</i> , <i>Gstm2</i> , <i>Fcgrt</i> , <i>Prdx5</i> , <i>Fmod</i> , <i>Crif1</i> , <i>Prelp</i> , <i>Svep1</i> , <i>Plac8</i> , <i>Heph</i> , <i>Swap70</i> , <i>Mxra8</i> , <i>Sdc2</i> , <i>Colec12</i> , <i>Pcolce2</i> , <i>Flt4</i> , <i>Gbp1</i> , <i>Hck</i> , <i>Dusp14</i> , <i>Cd109</i> , <i>Ptpre</i>
Cell adhesion	1.33E-05	3.05	19	6.22	<i>Dner</i> , <i>Cd55</i> , <i>Lama2</i> , <i>Fmod</i> , <i>Prelp</i> , <i>Svep1</i> , <i>Plac8</i> , <i>Heph</i> , <i>Mxra8</i> , <i>Sdc2</i> , <i>Colec12</i> , <i>Pcolce2</i> , <i>Flt4</i> , <i>Hck</i> , <i>Ptpre</i> , <i>Rerg</i> , <i>Vcan</i> , <i>Odz4</i> , <i>Rgnef</i>
Cell communication	1.65E-05	1.89	41	21.72	<i>Dner</i> , <i>Cd55</i> , <i>Lama2</i> , <i>Fmod</i> , <i>Prelp</i> , <i>Svep1</i> , <i>Heph</i> , <i>Sdc2</i> , <i>Colec12</i> , <i>Pcolce2</i> , <i>Flt4</i> , <i>Hck</i> , <i>Ptpre</i> , <i>Rerg</i> , <i>Vcan</i> , <i>Odz4</i> , <i>Rgnef</i> , <i>Thbd</i> , <i>Cxcr7</i> , <i>Hunk</i> , <i>Crif1</i> , <i>Dusp14</i> , <i>Cd109</i> , <i>Rcan2</i> , <i>Socs3</i> , <i>Fam43a</i> , <i>Trib2</i> , <i>Grk5</i> , <i>Tpcn1</i> , <i>Avpr1a</i> , <i>Fgf7</i> , <i>Acvr2a</i> , <i>Figf</i> , <i>Myh3</i> , <i>Tob1</i> , <i>Acvr11</i> , <i>Moxd1</i> , <i>Tgfb3</i> , <i>Lpp</i> , <i>Wnt4</i>
Development	4.81E-05	2.11	30	14.22	<i>Dner</i> , <i>Lama2</i> , <i>Fmod</i> , <i>Prelp</i> , <i>Heph</i> , <i>Sdc2</i> , <i>Colec12</i> , <i>Pcolce2</i> , <i>Flt4</i> , <i>Ebf1</i> , <i>Hck</i> , <i>Ptpre</i> , <i>Vcan</i> , <i>Odz4</i> , <i>Thbd</i> , <i>Hunk</i> , <i>Crif1</i> , <i>Rcan2</i> , <i>Socs3</i> , <i>Avpr1a</i> , <i>Fgf7</i> , <i>Figf</i> , <i>Myh3</i> , <i>Tgfb3</i> , <i>Lpp</i> , <i>Klf4</i> , <i>Cebpa</i> , <i>Cebpb</i> , <i>Hoxa5</i> , <i>Hoxb5</i> , <i>Irx5</i>
Metabolism	1.91E-03	1.38	57	41.44	<i>Dner</i> , <i>Heph</i> , <i>Pcolce2</i> , <i>Flt4</i> , <i>Hck</i> , <i>Ptpre</i> , <i>Odz4</i> , <i>Hunk</i> , <i>Klf4</i> , <i>Cebpa</i> , <i>Cebpb</i> , <i>Hoxa5</i> , <i>Hoxb5</i> , <i>Irx5</i> , <i>Cd55</i> , <i>Svep1</i> , <i>Rgnef</i> , <i>Dusp14</i> , <i>Cd109</i> , <i>Trib2</i> , <i>Grk5</i> , <i>Acvr2a</i> , <i>Acvr11</i> , <i>Moxd1</i> , <i>Prdx5</i> , <i>Swap70</i> , <i>Satb1</i> , <i>Amacr</i> , <i>Dhrs3</i> , <i>Ell2</i> , <i>Npr3</i> , <i>Man2a1</i> , <i>Prkd1</i> , <i>Cyp1b1</i> , <i>Serpib1a</i> , <i>Chst1</i> , <i>Hsd3b7</i> , <i>Aldh1a7</i> , <i>H6pd</i> , <i>Serpine2</i> , <i>Cyp7b1</i> , <i>P4ha2</i> , <i>Larp6</i> , <i>Mrps11</i> , <i>Aox1</i> , <i>Hdac5</i> , <i>Cpxm1</i> , <i>Eno2</i> , <i>Sox11</i> , <i>Prkcdpb</i> , <i>Ccrn4</i> , <i>Erc1</i> , <i>Pqlc3</i> , <i>Bcl11b</i>

Biological processes enriched in cohesin target genes with cohesin binding at either promoters or gene regions. "Gene number" is the number of cohesin target genes that belong to a specific category; "Expected number" is the expected gene numbers that belong to a specific category at random



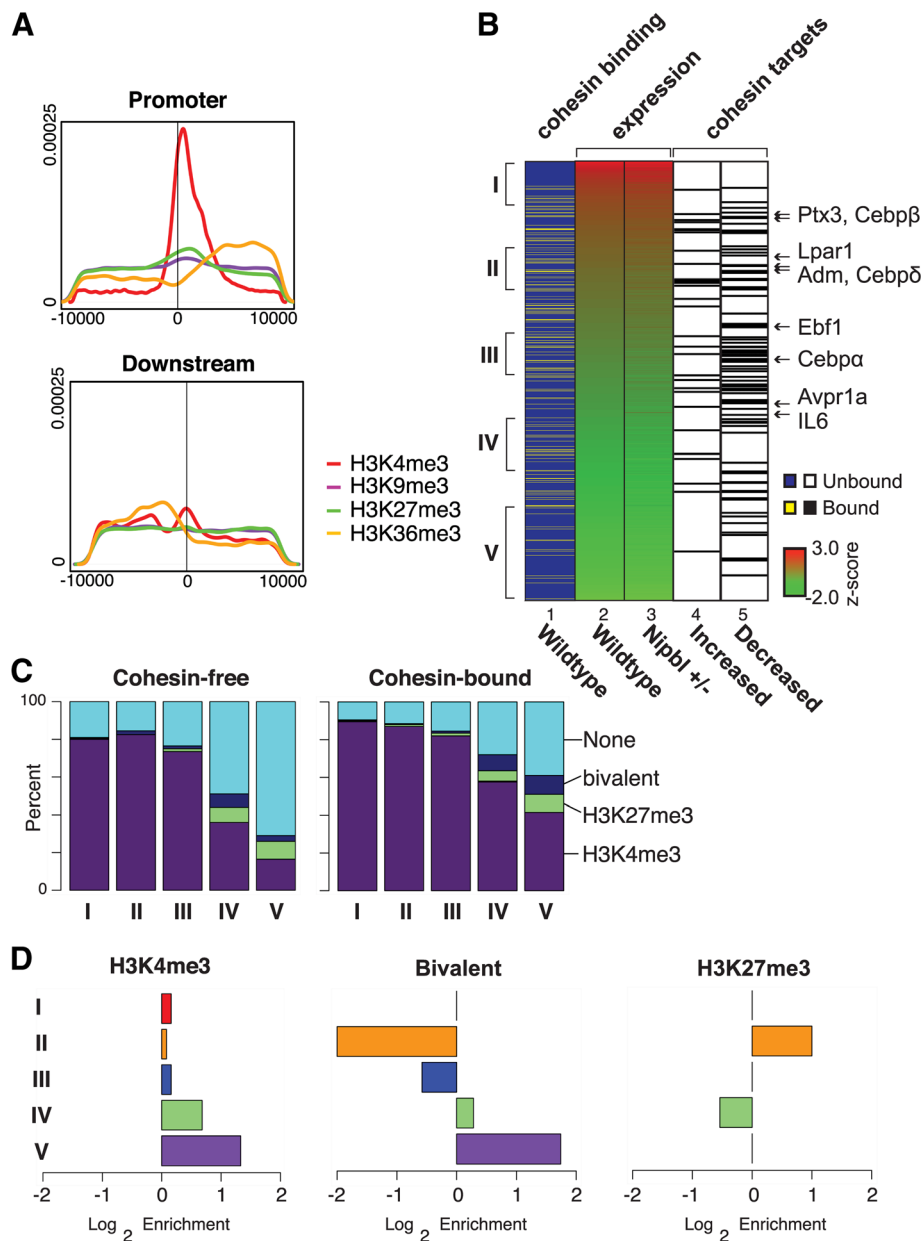
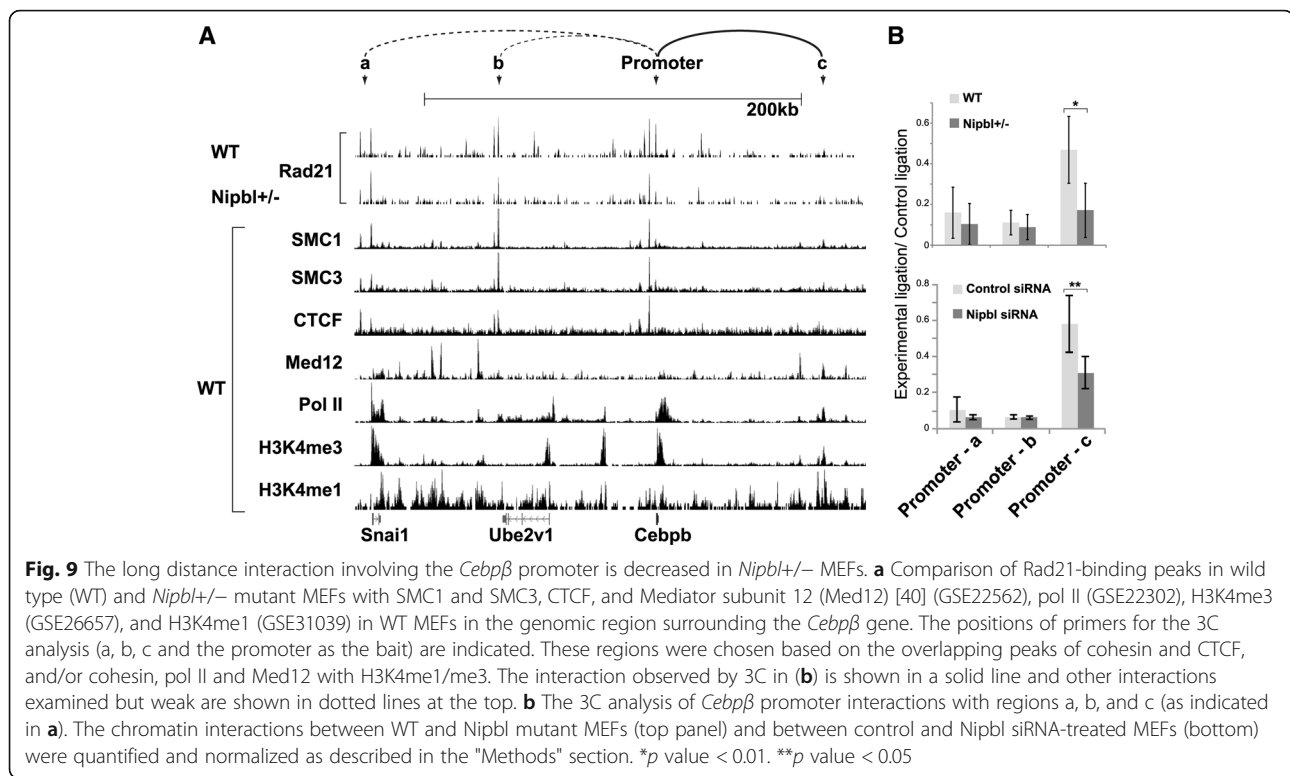


Fig. 8 Enrichment of H3K4me3 at the promoters of cohesin-bound genes. **a** Density of histone modifications within 10 kb of cohesin peaks found in the promoter or downstream regions. Histone methylation data was downloaded from NCBI (GEO: GSE26657). Tags within a 10-kb window around cohesin peaks located in a promoter region were counted and normalized to the total number of tags (reads per million) and used to generate a density plot. **b** Expression status of cohesin target genes. Genes are ranked by their expression status (shown as a z-score) in wild type MEFs (lane 2), and those genes with cohesin binding at the promoter regions are indicated by yellow lines (lane 1). The expression status of the corresponding genes in *Nipbl* mutant cells is also shown (lane 3), and the cohesin target genes (Table 2) (either upregulated (lane 4) or downregulated (lane 5) in mutant cells) are indicated by black lines. Genes in the adipogenesis pathway are indicated with arrows on the right. Five clusters (I through V) of 200 cohesin-bound genes each in wild type MEFs according to the expression levels are indicated on the left, which were used for the analysis in **c** and **d**. **c** The numbers of cohesin target genes containing histone marks in the promoter were tallied for the categories I through V from **b**. As a control, the cohesin-free gene directly below each cohesin target gene was also tallied and plotted. H3K4me3, H3K9me3, H3K27me3, bivalent (H3K4me3 and H3K27me3), and the promoters with none of these marks (“None”) are indicated. There is almost no signal of H3K9me3 in these categories. **d** Enrichment plot of H3K4me3, H3K27me3, and bivalent (H3K4me3 and K27me3) in promoters of cohesin-bound genes versus cohesin-free genes in the five expression categories as in **c** is shown



Nipbl reduction. The results indicate that the decrease of long-distance chromatin interaction involving the promoters and distant DNA elements is one of the direct consequences of reduced cohesin binding, which may be one mechanism of gene expression alteration by *Nipbl* haploinsufficiency.

Discussion

In this study, we used MEFs derived from *Nipbl* heterozygous mutant mice to analyze the effect of *Nipbl* haploinsufficiency (the primary cause of CdLS) on cohesin binding and its relationship to gene expression. We found a genome-wide decrease in cohesin binding even at CTCF sites and repeat regions, indicating the high sensitivity of cohesin binding to even a partial reduction of the *Nipbl* protein. Importantly, the expression of genes bound by cohesin, particularly at the promoter regions, is preferentially altered in response to *Nipbl* reduction. While some genes are activated, the majority of cohesin-bound genes are repressed by decreased cohesin binding, indicating the positive role of cohesin in this context. This is consistent with the significant enrichment of H3K4me3 at the promoters of cohesin-bound genes. Our results indicate that more than 50% of genes whose expression is altered significantly in *Nipbl* haploinsufficient cells are cohesin target genes directly influenced by decreased cohesin binding at the individual gene regions. One consequence of reduced cohesin

binding at the promoter region is a decrease of a specific long-distance chromatin interaction, raising the possibility that cohesin-dependent higher-order chromatin organization in the nucleus may be globally altered in CdLS patient cells.

Nipbl functions in cohesin loading at both CTCF and non-CTCF sites

In mESCs, it was suggested that *Nipbl* is involved in cohesin binding to only a subset of cohesin-binding sites, which are largely distinct from CTCF-bound sites [40]. However, we found that *Nipbl* binds to, and its haploinsufficiency decreased cohesin binding to, CTCF sites in MEFs. A similar decrease of cohesin binding was observed at both CTCF insulators and non-CTCF sites in the *β-globin* locus in *Nipbl*^{+/-} fetal mouse liver [35]. Furthermore, during differentiation in mouse erythroleukemia cells, both *Nipbl* and cohesin binding is concomitantly increased at these sites [35]. Therefore, while cohesin was suggested to slide from the *Scs2* (*Nipbl* homolog)-dependent loading sites in yeast [79, 80], *Nipbl* is present and appears to directly affect cohesin loading at CTCF sites in mammalian cells. *Nipbl*, rather than cohesin, interacts with Mediator and HP1 and appears to recruit and load cohesin onto genomic regions enriched for Mediator and HP1 for gene activation and heterochromatin assembly, respectively [40, 45]. In contrast, cohesin, and not *Nipbl*, primarily interacts with

CTCF [45, 81]. Thus, for cohesin binding to CTCF sites, we envision that cohesin initially recruits Nipbl that in turn stably loads cohesin onto CTCF sites.

A recent study indicated that almost all CTCF sites are bound by cohesin in primary mouse liver [43]. In MEFs, however, we found that ~42% of CTCF-bound sites appear to be cohesin-free. Furthermore, there is less overlap of cohesin and CTCF in the promoter regions compared to the intergenic regions, and little correlation between CTCF binding to the promoter and gene expression changes in *Nipbl* mutant cells was observed. Thus, in contrast to the cooperative function of cohesin and CTCF at distantly located insulator sites [36], cohesin and CTCF appear to have distinct functions at gene promoters. Distinct gene regulatory functions of CTCF and cohesin have also been reported in human cells [41]. Further study is needed to understand the recruitment specificity and functional relationship of cohesin and CTCF in gene regulation.

How does Nipbl haploinsufficiency affect cohesin target gene expression?

One mechanism of cohesin action in gene regulation is to mediate chromatin loop formation [35, 40]. Increased Nipbl and cohesin binding correlates with the induction of the enhancer-promoter interaction and robust gene activation at the β -globin locus [35]. Depletion of cohesin resulted in decreased enhancer-promoter interactions and downregulation of globin genes [35]. Similarly, *Nipbl* haploinsufficiency results in less cohesin binding and decreased promoter-enhancer interactions and β -globin gene expression [35]. In the current study, we also found that the cohesin-bound promoter of one of the target genes, *Cebpb*, is involved in a long-distance chromatin interaction with a putative enhancer, which is decreased in *Nipbl* mutant cells, consistent with the decreased gene expression. Thus, *Nipbl* haploinsufficiency affects cohesin target gene expression by decreasing cohesin-mediated chromatin interactions.

It should be noted, however, that not all genes that we examined showed significant long-distance chromatin interactions involving cohesin-bound promoters. While this may be because we did not test the correct enhancer regions, it also suggests that cohesin may promote gene activation by a mechanism(s) other than by mediating long-distance promoter interaction. One possibility is gene looping. In *Saccharomyces cerevisiae*, the promoter and terminator regions of genes interact with each other, which was thought to facilitate transcription re-initiation [82]. Although cohesin is often found at the promoter and terminator regions of genes in MEFs, we failed to obtain any evidence for the involvement of these sites in gene looping with our limited analysis. Thus, how (or whether) cohesin at the promoter may regulate gene

transcription in a loop formation-independent manner is currently unclear.

Cohesin binding to the gene body regions is found at many of the cohesin target genes. This may represent the cohesin binding at intragenic enhancer elements or may be related to Pol II pausing [29]. While cohesin was shown to facilitate Pol II elongation in *Drosophila* [83–85], cohesin together with CTCF in the intragenic region was found to cause Pol II pausing at the *PUMA* gene in human cells [86], suggesting that cohesin can have both positive and negative effects on transcriptional elongation in a context-dependent manner. Furthermore, not all the cohesin-bound genes changed expression in *Nipbl*^{+/-} MEFs, echoing this notion that the effect of cohesin binding on gene expression is context-dependent. What determines the effects of cohesin binding at individual binding sites on gene expression requires further investigation.

The role of cohesin in the maintenance of gene expression

While there is now strong evidence for cohesin's role in chromatin organization and gene activation, whether cohesin is involved in initiation or maintenance of gene activation is less clear. Enrichment of cohesin binding at the transcription start sites and termination sites was observed previously in mouse immune cells with no significant correlation to gene expression [30]. Our genome-wide analysis also revealed that cohesin binding to the gene regions has no obvious relationship to the level of gene expression in wild type MEFs. And yet, a decrease in cohesin binding is associated with a tendency to downregulate these genes, indicative of the positive role of cohesin on gene expression, consistent with the enriched presence of H3K4me3 in promoter regions. We speculate that cohesin may not be the primary determinant of gene activation, but rather cohesin binding may be important for maintaining gene expression status initially determined by sequence- and cell type-specific transcription factors. Similarly, enrichment of bivalent histone modifications in the promoters of cohesin-bound genes with very low expression suggests that cohesin also contributes to the maintenance of the poised state of these genes.

Nipbl haploinsufficiency vs. cohesin mutation

There are two different cohesin complexes in mammalian somatic cells that differ by one non-SMC subunit (i.e., SA1 (STAG1) or SA2 (STAG2)) [87, 88]. A recent report on SA1 knockout mice revealed some phenotypic similarity to what is seen in mice with *Nipbl* haploinsufficiency [67]. Interestingly, the *SA1* gene is one of the cohesin target genes that is slightly upregulated in *Nipbl* mutant cells [19]. Thus, together with the compensatory increase of *Nipbl* expression from the intact allele, there

appears to be a feedback mechanism that attempts to balance the expression of *Nipbl* and cohesin in response to *Nipbl* mutation. The fact that upregulation was observed with the *SA1*, but not *SA2*, gene may reflect the unique transcriptional role of *SA1* [67]. Interestingly, however, only 10% of genes altered in *Nipbl* mutant MEFs are changed significantly in *SA1* KO MEFs [67]. This discrepancy may, as observed in *Drosophila* [89], reflect the different effects of decreased binding versus complete knockout of a cohesin subunit on target gene expression. It could also be a result of the decreased binding of the second cohesin complex, cohesin-*SA2*.

Cohesin binding was relatively uniformly decreased genome-wide in *Nipbl* haploinsufficient cells with no significant redistribution of cohesin-binding sites. Point mutations of different subunits of cohesin cause CdLS and CdLS-like disorders with both overlapping and distinct phenotypes compared to CdLS cases caused by NIPBL mutations [9, 10, 13]. Non-overlapping effects of downregulation of different cohesin subunits have been reported in zebrafish [20, 26]. This may reflect an unequal role of each cohesin subunit in gene regulation, and it is possible that some of the cohesin target genes may be particularly sensitive to a specific cohesin subunit mutation. For example, similar to the TBP-associating factors (TAFs) in TFIID [90], cohesin subunits may provide different interaction surfaces for distinct transcription factors, which would dictate their differential recruitment and/or transcriptional activities. Furthermore, recent studies provide evidence for cohesin-independent roles of NIPBL in chromatin compaction and gene regulation [27, 28, 91]. Thus, disturbance of cohesin functions as well as impairment of cohesin-independent roles of NIPBL may collectively contribute to CdLS caused by NIPBL mutations.

Conclusions

Our results demonstrate that cohesin binding to chromatin is highly sensitive genome-wide (both at unique and repeat regions) to partial *Nipbl* reduction, resulting in a general decrease in cohesin binding even at strong CTCF sites. Many genes whose expression is changed by *Nipbl* reduction are actual cohesin target genes. Our results suggest that decreased cohesin binding due to partial reduction of NIPBL at the gene regions directly contributes to disorder-specific gene expression changes and the CdLS phenotype. This work provides important insight into the function of cohesin in gene regulation with direct implications for the mechanism underlying *NIPBL* haploinsufficiency-induced CdLS pathogenesis.

Abbreviations

3C: Chromatin conformation capture (3C); CdLS: Cornelia de Lange syndrome; ChIP: Chromatin immunoprecipitation; CTCF: CCCCTC-binding factor; FDR: False discovery rate; H3K27me3: Histone H3 lysine 27

trimethylation; H3K4me1: Histone H3 lysine 4 monomethylation; H3K4me3: Histone H3 lysine 4 trimethylation; KS test: Kolmogorov-Smirnov test; MEFs: Mouse embryonic fibroblasts; mESCs: Mouse embryonic stem cells; Nipbl: Nipped-B-like; Pol II: RNA polymerase II; RPKM: Reads per kilobase per million total reads; siRNA: Small interfering RNA; TSS: Transcription start site; TTS: Transcription termination site

Acknowledgements

We thank Dr. Alex Ball for critical reading of the manuscript.

Funding

This work was supported in part by the National Institute of Health [HD052860 to A.D.L. and A.L.C., HG006870 and NSF IIS-1715017 to X.X., HD062951 to K.Y., T32 CA113265 to R.C., T15LM07443 to D.A.N., T32 CA09054 to Y.Y.C.] and the California Institute of Regenerative Medicine [TB1-01182 to E.F].

Availability of data and materials

The datasets used and/or analyzed during the current study are available from the corresponding author on a reasonable request.

Authors' contributions

KY and XX conceived the idea, designed experiments, and analyzed and interpreted the data. ALC and ADL contributed to designing experiments and data analysis. SK and RS prepared the samples. YYC and RC as well as WZ and EF performed experiments/data acquisition. DAN, JB, RC, and YYC performed data analysis. DAN, YYC, RC, ADL, XX, and KY wrote the manuscript. All authors read and approved the final manuscript.

Consent for publication

Not applicable.

Ethics approval and consent to participate

Not applicable

Competing interests

The authors declare that they have no competing interests.

Publisher's Note

Springer Nature remains neutral with regard to jurisdictional claims in published maps and institutional affiliations.

Author details

¹Department of Biological Chemistry, School of Medicine, University of California, Irvine, CA 92697, USA. ²Department of Computer Sciences, University of California, Irvine, CA 92697, USA. ³Department of Anatomy & Neurobiology, School of Medicine, University of California, Irvine, CA 92697, USA. ⁴Department of Developmental & Cell Biology, School of Biological Sciences, University of California, Irvine, CA 92697, USA. ⁵California State University Long Beach, Long Beach, CA 90840, USA. ⁶Current address: ResearchDx Inc., 5 Mason, Irvine, CA 92618, USA. ⁷Current address: Thermo Fisher Scientific, Inc., 180 Oyster Point Blvd South, San Francisco, CA 94080, USA. ⁸Current address: Department of Developmental & Cell Biology, School of Biological Sciences, University of California, Irvine, CA 92697, USA. ⁹Current address: Verily Life Sciences, 1600 Amphitheatre Pkwy, Mountain View, CA 94043, USA. ¹⁰Current address: UT Southwestern Medical Center, 5323 Harry Hines Blvd, NA8.124, Dallas, TX 75390, USA.

Received: 22 May 2017 Accepted: 15 August 2017

Published online: 25 August 2017

References

- DeScipio C, Kaur M, Yaeger D, Innis JW, Spinner NB, Jackson LG, Krantz ID. Chromosome rearrangements in cornelia de Lange syndrome (CdLS): report of a der(3) t(3;12)(p25.3;p13.3) in two half sibs with features of CdLS and review of reported CdLS cases with chromosome rearrangements. *Am J Med Genet.* 2005;137:276–82.
- Liu J, Krantz ID. Cornelia de Lange syndrome, cohesin, and beyond. *Clin Genet.* 2009;76:303–14.
- Krantz ID, McCallum J, DeScipio C, Kaur M, Gillis LA, Yaeger D, Jukofsky L, Wasserman N, Bottani A, Morris CA, et al. Cornelia de Lange syndrome is

- caused by mutations in NIPBL, the human homolog of *Drosophila melanogaster* Nipped-B. *Nat Genet.* 2004;36:631–5.
4. Tonkin ET, Wang TJ, Ligo S, Bamshad MJ, Strachan T. NIPBL, encoding a homolog of fungal Scc2-type sister chromatid cohesion proteins and fly Nipped-B, is mutated in Cornelia de Lange syndrome. *Nat Genet.* 2004;36:636–41.
 5. Ciosk R, Shirayama M, Shevchenko A, Tanaka T, Toth A, Shevchenko A, Nasmyth K. Cohesin's binding to chromosomes depends on a separate complex consisting of Scc2 and Scc4 proteins. *Mol Cell.* 2000;5:243–54.
 6. Chien R, Zeng W, Ball AR, Yokomori K. Cohesin: a critical chromatin organizer in mammalian gene regulation. *Biochem Cell Biol.* 2011;89:445–58.
 7. Dorsett D, Ström L. The ancient and evolving roles of cohesin in gene expression and DNA repair. *Curr Biol.* 2012;22
 8. Nasmyth K, Haering CH. Cohesin: its roles and mechanisms. *Annu Rev Genet.* 2009;43:525–8.
 9. Musio A, Selicorni A, Focarelli ML, Gervasini C, Milani D, Russo S, Vezzoni P, Larizza L. X-linked Cornelia de Lange syndrome owing to SMC1L1 mutations. *Nat Genet.* 2006;38:528–30.
 10. Deardorff MA, Kaur M, Yaeger D, Rampuria A, Korolev S, Pie J, Gil-Rodríguez C, Arnedo M, Loeyes B, Kline AD, et al. Mutations in cohesin complex members SMC3 and SMC1A cause a mild variant of cornelia de Lange syndrome with predominant mental retardation. *Am J Hum Genet.* 2007;80:485–94.
 11. Mannini L, Menga S, Tonelli A, Zanotti S, Bassi MT, Magnani C, Musio A. SMC1A codon 496 mutations affect the cellular response to genotoxic treatments. *Am J Med Genet.* 2012;158A:224–8.
 12. Deardorff MA, Bando M, Nakato R, Watrin E, Itoh T, Minamino M, Saitoh K, Komata M, Katou Y, Clark D, et al. HDAC8 mutations in Cornelia de Lange syndrome affect the cohesin acetylation cycle. *Nature.* 2012;489:313–7.
 13. Deardorff MA, Wilde JJ, Albrecht M, Dickinson E, Tenstedt S, Braunholz D, Mönnich M, Yan Y, Xu W, Gil-Rodríguez MC, et al. RAD21 mutations cause a human cohesinopathy. *Am J Hum Genet.* 2012;90:1014–27.
 14. Castronovo P, Delahaye-Duriez A, Gervasini C, Azzollini J, Minier F, Russo S, Masciadri M, Selicorni A, Verloes A, Larizza L. Somatic mosaicism in Cornelia de Lange syndrome: a further contributor to the wide clinical expressivity? *Clin Genet.* 2010;78:560–4.
 15. Dorsett D, Krantz ID. On the molecular etiology of Cornelia de Lange syndrome. *Ann N Y Acad Sci.* 2009;1151:22–37.
 16. Selicorni A, Russo S, Gervasini C, Castronovo P, Milani D, Cavalleri F, Bentivegna A, Masciadri M, Dorni A, Divizia MT, et al. Clinical score of 62 Italian patients with Cornelia de Lange syndrome and correlations with the presence and type of NIPBL mutation. *Clin Genet.* 2007;72:98–108.
 17. Borck G, Zarhrate M, Cluzeau C, Bal E, Bonnefont JP, Munnich A, Cormier-Daire V, Colleaux L. Father-to-daughter transmission of Cornelia de Lange syndrome caused by a mutation in the 5' untranslated region of the NIPBL Gene. *Hum Mutat.* 2006;27(8):731–5.
 18. Liu J, Zhang Z, Bando M, Itoh T, Deardorff MA, Clark D, Kaur M, Tandy S, Kondoh T, Rappaport E, et al. Transcriptional dysregulation in NIPBL and cohesin mutant human cells. *PLoS Biol.* 2009;7:e1000119.
 19. Kawauchi S, Calof AL, Santos R, Lopez-Burks ME, Young CM, Hoang MP, Chua A, Lao T, Lechner MS, Daniel JA, et al. Multiple organ system defects and transcriptional dysregulation in the Nipbl(+/-) mouse, a model of Cornelia de Lange syndrome. *PLoS Genet.* 2009;5:e1000650.
 20. Horsfield JA, Print CG, Mönnich M. Diverse developmental disorders from the one ring: distinct molecular pathways underlie the cohesinopathies. *Front Genet.* 2012;3:171.
 21. Dorsett D. Cohesin: genomic insights into controlling gene transcription and development. *Curr Opin Genet Dev.* 2011;21:199–206.
 22. Kaur M, Descipio C, McCallum J, Yaeger D, Devoto M, Jackson LG, Spinner NB, Krantz ID. Precocious sister chromatid separation (PSCS) in Cornelia de Lange syndrome. *Am J Med Genet.* 2005;138:27–31.
 23. Castronovo P, Gervasini C, Cereda A, Masciadri M, Milani D, Russo S, Selicorni A, Larizza L. Premature chromatid separation is not a useful diagnostic marker for Cornelia de Lange syndrome. *Chromosom Res.* 2009;17(6):763–71.
 24. Vrouwe MG, Elghalbzouri-Maghrani E, Meijers M, Schouten P, Godthelp BC, Bhuiyan ZA, Redeker EJ, Mannens MM, Mullenders LH, Pastink A, et al. Increased DNA damage sensitivity of Cornelia de Lange syndrome cells: evidence for impaired recombinational repair. *Hum Mol Genet.* 2007;16:1478–87.
 25. Mannini L, Cucco F, Quarantotti V, Krantz ID, Musio A. Mutation spectrum and genotype-phenotype correlation in Cornelia de Lange syndrome. *Hum Mutat.* 2013;34:1589–96.
 26. Muto A, Calof AL, Lander AD, Schilling TF. Multifactorial origins of heart and gut defects in nipbl-deficient zebrafish, a model of Cornelia de Lange Syndrome. *PLoS Biol.* 2011;9:e1001181.
 27. Yuen KC, Xu B, Krantz ID, Gerton JL. NIPBL controls RNA biogenesis to prevent activation of the stress kinase PKR. *Cell Rep.* 2016;14:93–102.
 28. Zuin J, Franke V, van Ijcken WF, van der Sloot A, Krantz ID, van der Reijden MI, Nakato R, Lenhard B, Wendt KS. A cohesin-independent role for NIPBL at promoters provides insights in CdLS. *PLoS Genet.* 2014;10:e1004153.
 29. Ball AR Jr, Chen YY, Yokomori K. Mechanisms of cohesin-mediated gene regulation and lessons learned from cohesinopathies. *BBA Gene Regul Mech.* 2014;1839:191–202.
 30. Parelho V, Hadjur S, Spivakov M, Leleu M, Sauer S, Gregson HC, Jarmuz A, Canzonetta C, Webster Z, Nesterova T, et al. Cohesins functionally associate with CTCF on mammalian chromosome arms. *Cell.* 2008;132:422–33.
 31. Wendt KS, Yoshida K, Itoh T, Bando M, Koch B, Schirghuber E, Tsutsumi S, Nagae G, Ishihara K, Mishiro T, et al. Cohesin mediates transcriptional insulation by CCCTC-binding factor. *Nature.* 2008;451:796–801.
 32. Rubio ED, Reiss DJ, Welch PL, Distecher CM, Filippova GN, Baliga NS, Aebersold R, Ranish JA, Krumm A. CTCF physically links cohesin to chromatin. *Proc Natl Acad Sci.* 2008;105:8309–14.
 33. Stedman W, Kang H, Lin S, Kissil JL, Bartolomei MS, Lieberman PM. Cohesins localize with CTCF at the KSHV latency control region and at cellular c-myc and H19/Igf2 insulators. *EMBO J.* 2008;27:654–66.
 34. Zlatanova J, Caiafa P. CTCF and its protein partners: divide and rule? *J Cell Sci.* 2009;122:1275–84.
 35. Chien R, Zeng W, Kawauchi S, Bender MA, Santos R, Gregson HC, Schmiesing JA, Newkirk D, Kong X, Ball ARJ, et al. Cohesin mediates chromatin interactions that regulate mammalian β -globin expression. *J Biol Chem.* 2011;286:17870–8.
 36. Hadjur S, Williams LM, Ryan NK, Cobb BS, Sexton T, Fraser P, Fisher AG, Merkenschlager M. Cohesins form chromosomal cis-interactions at the developmentally regulated IFNG locus. *Nature.* 2009;460:410–3.
 37. Mishiro T, Ishihara K, Hino S, Tsutsumi S, Aburatani H, Shirahige K, Kinoshita Y, Nakao M. Architectural roles of multiple chromatin insulators at the human apolipoprotein gene cluster. *EMBO J.* 2009;28:1234–45.
 38. Nativio R, Wendt KS, Ito Y, Huddleston JE, Uribe-Lewis S, Woodfine K, Krueger C, Reik W, Peters JM, Murrell A. Cohesin is required for higher-order chromatin conformation at the imprinted IGF2-H19 locus. *PLoS Genet.* 2009;5:e1000739.
 39. Phillips-Cremins JE, Sauria ME, Sanyal A, Gerasimova TI, Lajoie BR, Bell JS, Ong CT, Hookway TA, Guo C, Sun Y, et al. Architectural protein subclasses shape 3D organization of genomes during lineage commitment. *Cell.* 2013; doi:https://doi.org/10.1016/j.cell.2013.04.053.
 40. Kagey MH, Newman JJ, Bilodeau S, Zhan Y, Orlando DA, van Berkum NL, Ebmeier CC, Goossens J, Rahl PB, Levine SS, et al. Mediator and cohesin connect gene expression and chromatin architecture. *Nature.* 2010;467:430–5.
 41. Zuin J, Dixon JR, van der Reijden MI, Ye Z, Kolovos P, Brouwer RW, van de Corput MP, van de Werken HJ, Knoch TA, van Ijcken WF et al.: Cohesin and CTCF differentially affect chromatin architecture and gene expression in human cells. *Proc Natl Acad Sci* 2014, 111:996–1001.
 42. Schmidt D, Schwalie P, Ross-Innes CS, Hurtado A, Brown G, Carroll J, Flicek P, Odom D. A CTCF-independent role for cohesin in tissue-specific transcription. *Genome Res.* 2010;20:578–88.
 43. Faure AJ, Schmidt D, Watt S, Schwalie PC, Wilson MD, Xu H, Ramsay RG, Odom DT, Flicek P. Cohesin regulates tissue-specific expression by stabilizing highly occupied cis-regulatory modules. *Genome Res.* 2012;22:2163–75.
 44. Shimura M, Toyoda Y, Iijima K, Kinomoto M, Tokunaga K, Yoda K, Yanagida M, Sata T, Ishizaka Y. Epigenetic displacement of HP1 from heterochromatin by HIV-1 Vpr causes premature sister chromatid separation. *J Cell Biol.* 2011; 194:721–35.
 45. Zeng W, de Greef JC, Chen Y-Y, Chien R, Kong X, Gregson HC, Winokur ST, Pyle A, Robertson KD, Schmiesing JA, et al. Specific loss of histone H3 lysine 9 trimethylation and HP1 γ /cohesin binding at D4Z4 repeats is associated with facioscapulohumeral dystrophy (FSHD). *PLoS Genet.* 2009;5:e1000559.
 46. Gregson HC, Schmiesing JA, Kim J-S, Kobayashi T, Zhou S, Yokomori K. A potential role for human cohesin in mitotic spindle aster assembly. *J Biol Chem.* 2001;276:47575–82.
 47. Langmead B, Trapnell C, Pop M, Salzberg SL. Ultrafast and memory-efficient alignment of short DNA sequences to the human genome. *Genome Biol.* 2009;10:R25.

48. Martens JH, O'Sullivan RJ, Braunschweig U, Opravil S, Radolf M, Steinlein P, Jenuwein T. The profile of repeat-associated histone lysine methylation states in the mouse epigenome. *EMBO J*. 2005;24:800–12.
49. Zeng W, Chen YY, Newkirk DA, Wu B, Balog J, Kong X, Ball AR Jr, Zanotti S, Tawil R, Hashimoto N, et al. Genetic and epigenetic characteristics of FSHD-associated 4q and 10q D4Z4 that are distinct from non-4q/10q D4Z4 homologs. *Hum Mutat*. 2014;35:998–1010.
50. Newkirk D, Biesinger J, Chon A, Yokomori K, Xie X. AREM: aligning short reads from ChIP-sequencing by expectation maximization. *J Comput Biol*. 2011;18:495–505.
51. Schmidt D, Schwalie PC, Wilson MD, Ballester B, Gonçalves A, Kutter C, Brown GD, Marshall A, Flicek P, Odom DT. Waves of retrotransposon expansion remodel genome organization and CTCF binding in multiple mammalian lineages. *Cell*. 2012;148:335–48.
52. Dale RK, Pedersen BS, Quinlan AR. Pybedtools: a flexible Python library for manipulating genomic datasets and annotations. *Bioinformatics*. 2011;27:3423–4.
53. Quinlan AR, Hall IM. BEDTools: a flexible suite of utilities for comparing genomic features. *Bioinformatics*. 2010;26:841–2.
54. Dean CB, Nielsen JD. Generalized linear mixed models: a review and some extensions. *Lifetime Data Anal*. 2007;13(4):497–512.
55. Rhead B, Karolchik D, Kuhn RM, Hinrichs AS, Zweig AS, Fujita PA, Diekhans M, Smith KE, Rosenbloom KR, Raney BJ, et al. The UCSC genome browser database: update 2010. *Nucleic Acids Res*. 2010;38(Database issue):D613–9.
56. Kent WJ, Sugnet CW, Furey TS, Roskin KM, Pringle TH, Zahler AM, Haussler D. The human genome browser at UCSC. *Genome Res*. 2002;12:996–1006.
57. Bailey TL, Elkan C. Fitting a mixture model by expectation maximization to discover motifs in biopolymers. *Proc Int Conf Intell Syst Mol Biol*. 1994;2:28–36.
58. Long AD, Mangalam HJ, Chan BY, Tollerli L, Hatfield GW, Baldi P. Improved statistical inference from DNA microarray data using analysis of variance and a Bayesian statistical framework. Analysis of global gene expression in *Escherichia coli* K12. *J Biol Chem*. 2001;276:19937–44.
59. Thomas PD, Kejarival A, Campbell MJ, Mi H, Diemer K, Guo N, Ladunga I, Ulitsky-Lazareva B, Muruganujan A, Rabkin S, et al. PANTHER: a browsable database of gene products organized by biological function, using curated protein family and subfamily classification. *Nuc Acids Res*. 2003;31:334–41.
60. Thomas PD, Kejarival A, Guo N, Mi H, Campbell MJ, Muruganujan A, Lazareva-Ulitsky B. Applications for protein sequence-function evolution data: mRNA/protein expression analysis and coding SNP scoring tools. *Nuc Acids Res*. 2006;34:W645–50.
61. Subramanian A, Tamayo P, Mootha VK, Mukherjee S, Ebert BL, Gillette MA, Paulovich A, Pomeroy SL, Golub TR, Lander ES, et al. Gene set enrichment analysis: a knowledge-based approach for interpreting genome-wide expression profiles. *Proc Natl Acad Sci*. 2005;102:15545–50.
62. Kampstra P. Beanplot: A Boxplot Alternative for Visual Comparison of Distributions. *J Stat Softw*. 2008; 28: <http://www.jstatsoft.org/v28/c01>.
63. Kooren J, Palstra RJ, Klous P, Splinter E, von Lindern M, Grosveld F, de Laat W. Beta-globin active chromatin Hub formation in differentiating erythroid cells and in p45 NF-E2 knock-out mice. *J Biol Chem*. 2007;282:16544–52.
64. Splinter E, Heath H, Kooren J, Palstra RJ, Klous P, Grosveld F, Galjart N, de Laat W. CTCF mediates long-range chromatin looping and local histone modification in the beta-globin locus. *Genes Dev*. 2006;20:2349–54.
65. Tolhuis B, Palstra RJ, Splinter E, Grosveld F, de Laat W. Looping and interaction between hypersensitive sites in the active beta-globin locus. *Mol Cell*. 2002;10:1453–65.
66. Hakimi MA, Bochar DA, Schmiesing JA, Dong Y, Barak OG, Speicher DW, Yokomori K, Shiekhattar R. A chromatin remodeling complex that loads cohesin onto human chromosomes. *Nature*. 2002;418:994–8.
67. Remeseiro S, Cuadrado A, Gómez-López G, Pisano DG, Losada A. A unique role of cohesin-SA1 in gene regulation and development. *EMBO J*. 2012;31:2090–102.
68. Mortazavi A, Williams BA, McCue K, Schaeffer L, Wold B. Mapping and quantifying mammalian transcriptomes by RNA-Seq. *Nat Methods*. 2008; 5:621–8.
69. Remeseiro S, Cuadrado A, Kawauchi S, Calof AL, Lander AD, Losada A. Reduction of Nipbl impairs cohesin loading locally and affects transcription but not cohesion-dependent functions in a mouse model of Cornelia de Lange syndrome. *Biochim Biophys Acta*. 1832;2013:2097–102.
70. Dunn KL, Davie JR. The many roles of the transcriptional regulator CTCF. *Biochem Cell Biol*. 2003;81:161–7.
71. Millau JF, Gaudreau L. CTCF, cohesin, and histone variants: connecting the genome. *Biochem Cell Biol*. 2011;89:505–13.
72. Misulovin Z, Schwartz YB, Li XY, Kahn TG, Gause M, MacArthur S, Fay JC, Eisen MB, Pirrotta V, Biggin MD, et al. Association of cohesin and Nipped-B with transcriptionally active regions of the *Drosophila melanogaster* genome. *Chromosoma*. 2008;117(1):89–102.
73. Kline AD, Barr M, Jackson LG. Growth manifestations in the Brachmann-de Lange syndrome. *Am J Med Genet*. 1993;47:1042–9.
74. Heintzman ND, Hon GC, Hawkins RD, Kheradpour P, Stark A, Harp LF, Ye Z, Lee LK, Stuart RK, Ching CW, et al. Histone modifications at human enhancers reflect global cell-type-specific gene expression. *Nature*. 2009; 459(7243):108–12.
75. Heintzman ND, Stuart RK, Hon G, Fu Y, Ching CW, Hawkins RD, Barrera LO, Van Calcar S, Qu C, Ching KA, et al. Distinct and predictive chromatin signatures of transcriptional promoters and enhancers in the human genome. *Nat Genet*. 2007;39:311–8.
76. Pekowska A, Benoukraf T, Zacarias-Cabeza J, Belhocine M, Koch F, Holota H, Imbert J, Andrau JC, Ferrier P, Spicuglia S. H3K4 tri-methylation provides an epigenetic signature of active enhancers. *EMBO J*. 2011;30:4198–210.
77. Sanborn AL, Rao SS, Huang SC, Durand NC, Huntley MH, Jewett AI, Bochkov ID, Chinnappan D, Cutkosky A, Li J, et al. Chromatin extrusion explains key features of loop and domain formation in wild-type and engineered genomes. *Proc Natl Acad Sci*. 2015;112:E6456–65.
78. de Wit E, Vos ES, Holwerda SJ, Valdes-Quezada C, Versteegen MJ, Teunissen H, Splinter E, Wijchers PJ, Krijger PH, de Laat W. CTCF binding polarity determines chromatin looping. *Mol Cell*. 2015;60:676–84.
79. Lengronne A, Katou Y, Mori S, Yokobayashi S, Kelly GP, Itoh T, Watanabe Y, Shirahige K, Uhlmann F. Cohesin relocation from sites of chromosomal loading to places of convergent transcription. *Nature*. 2004;430:573–8.
80. Ocampo-Hafalla MT, Uhlmann F. Cohesin loading and sliding. *J Cell Sci*. 2011;124:685–91.
81. Xiao T, Wallace J, Felsenfeld G. Specific sites in the C terminus of CTCF interact with the SA2 subunit of the cohesin complex and are required for cohesin-dependent insulation activity. *Mol Cell Biol*. 2011;31:2174–83.
82. Ansari A, Hampsey M. A role for the CPF 3'-end processing machinery in RNAP II-dependent gene looping. *Genes Dev*. 2005;19:2969–78.
83. Fay A, Misulovin Z, Li J, Schaaf CA, Gause M, Gilmour DS, Dorsett D. Cohesin selectively binds and regulates genes with paused RNA polymerase. *Curr Biol*. 2011;21:1624–34.
84. Misulovin Z, Schwartz YB, Li XY, Kahn TG, Gause M, MacArthur S, Fay JC, Eisen MB, Pirrotta V, Biggin MD, et al. Association of cohesin and Nipped-B with transcriptionally active regions of the *Drosophila melanogaster* genome. *Chromosoma*. 2008;117:89–102.
85. Schaaf CA, Kwak H, Koenig A, Misulovin Z, Gohara DW, Watson A, Zhou Y, Lis JT, Dorsett D. Genome-wide control of RNA polymerase II activity by cohesin. *PLoS Genet*. 2013;9:e1003382.
86. Gomes NP, Espinosa JM. Gene-specific repression of the p53 target gene PUMA via intragenic CTCF-Cohesin binding. *Genes Dev*. 2010;24(10):1022–34.
87. Losada A, Yokochi T, Kobayashi R, Hirano T. Identification and characterization of SA/Scp3p subunits in the *Xenopus* and human cohesin complexes. *J Cell Biol*. 2000;150:405–16.
88. Sumara I, Vorlaufer E, Gieffers C, Peters BH, Peters J-M. Characterization of vertebrate cohesin complexes and their regulation in prophase. *J Cell Biol*. 2000;151:749–61.
89. Schaaf CA, Misulovin Z, Sahota G, Siddiqui AM, Schwartz YB, Kahn TG, Pirrotta V, Gause M, Dorsett D. Regulation of the *Drosophila* Enhancer of split and invected-engrailed gene complexes by sister chromatid cohesion proteins. *PLoS One*. 2009;4:e6202.
90. Papai G, Weil PA, Schultz P. New insights into the function of transcription factor TFIIID from recent structural studies. *Curr Opin Genet Dev*. 2011;21:219–24.
91. Nolen LD, Boyle S, Ansari M, Pritchard E, Bickmore WA. Regional chromatin decompaction in Cornelia de Lange syndrome associated with NIPBL disruption can be uncoupled from cohesin and CTCF. *Hum Mol Genet*. 2013;22:4180–93.